Simulations of [7]Be and [10]Be with the GEOS-Chem global model v14.0.2 using state-of-the-art production rates

Minjie Zheng[1,2,3*], Hongyu Liu[4,5], Florian Adolphi[6,7], Raimund Muscheler[2], Zhengyao Lu[8], Mousong Wu[9], and Nønne L. Prisle[3*]

[1]Institute for Atmospheric and Climate Science, ETH Zürich, Zürich, Switzerland
[2]Department of Geology, Lund University, Lund, Sweden
[3]Center for Atmospheric Research, University of Oulu, Oulu, Finland
[4]National Institute of Aerospace, Hampton, Virginia, USA
[5]Science Directorate, NASA Langley Research Center, Hampton, Virginia, USA
[6]Alfred Wegener Institute, Helmholtz Centre for Polar and Marine Research, Bremerhaven, Germany
[7]Faculty of Geosciences, Bremen University, Bremen, Germany
[8]Department of Physical Geography and Ecosystem Science, Lund University, Lund, Sweden
[9]International Institute for Earth System Science, Nanjing University, Nanjing, China

Correspondence to: Minjie Zheng (minjie.zheng@env.ethz.ch) and Nønne L. Prisle (nonne.prisle@oulu.fi)

Abstract

The cosmogenic radionuclides [7]Be and [10]Be are useful aerosol tracers for atmospheric transport studies. Combining [7]Be and [10]Be measurements with an atmospheric transport model can not only improve our understanding of the radionuclide transport and deposition processes but also provide an evaluation of the transport process in the model. To simulate these aerosol tracers, it is critical to evaluate the influence of radionuclides production uncertainties on simulations. Here we use the GEOS-Chem chemical transport model driven by the MERRA-2 reanalysis to simulate [7]Be and [10]Be with different production scenarios: the default production rate in GEOS-Chem based on an empirical approach (denoted as LP67), and two production rates from the CRAC:Be (Cosmic Ray Atmospheric Cascade: Beryllium) model considering only geomagnetic cut-off rigidities for a geocentric axial dipole (denoted as P16) or realistic spatial geomagnetic cut-off rigidity variations due to non-dipole moments of the geomagnetic field (denoted as P16spa). The model results are comprehensively evaluated with a large number of measurements including surface air concentrations and deposition fluxes. The model with the P16spa production can reproduce the absolute values and temporal variability of [7]Be and [10]Be surface concentrations and deposition fluxes on annual and sub-annual scales, as well as the vertical profiles of air concentrations. Simulations with the LP67 production tend to overestimate the absolute values of [7]Be and [10]Be concentrations. The P16 simulations suggest less than 10% differences compared to P16spa but tend to produce a significant positive bias (>20%) in the [7]Be deposition fluxes over East Asia. We find that the deposition fluxes are more sensitive to the production in the troposphere and downward transport from the stratosphere. Independent of the production models, surface air concentrations and deposition fluxes from all simulations show similar seasonal variations, suggesting a dominant meteorological influence. The model can also reasonably simulate the stratosphere-troposphere exchange process of [7]Be and [10]Be by producing stratospheric contribution and [10]Be/[7]Be ratio values that agree with measurements. Finally, we illustrate the importance of including the time-varying solar modulation in the production calculation, which can significantly improve the agreement between model results and measurements, especially at mid- and high- latitudes. Reduced uncertainties in the production rates, as

40   demonstrated in this study, improve the utility of ^{7}Be and ^{10}Be as aerosol tracers for evaluating and testing transport and scavenging processes in global models.

1 Introduction

The naturally occurring cosmogenic radionuclide ^{7}Be (half-life of 53.3 days) is monitored worldwide and has been recognized as a useful tracer in atmospheric dynamic studies (Aldahan et al., 2001; Hernández-Ceballos et

45   al., 2016; Terzi et al., 2019; Liu et al., 2016). Especially, ratios of radionuclides concentrations with very different half-lives, such as the ^{10}Be/^{7}Be ratio, have become powerful tools (e.g., Liu et al., 2022b; Raisbeck et al., 1981) to disentangle the influence of transport and deposition since both ^{7}Be and ^{10}Be from the troposphere are removed by the wet deposition. In this paper, we aim to improve the utility of ^{7}Be and ^{10}Be as tracers for atmospheric transport by using state-of-the-art production rates in a global 3-D chemical transport model.

50   ^{7}Be and ^{10}Be are produced through interactions between atmospheric atoms and incoming galactic cosmic rays (GCRs) in the atmosphere (Lal and Peters, 1967, referred to as LP67 hereafter; Poluianov et al., 2016, referred to as P16 hereafter). Due to the atmospheric depth-profile of fluxes of primary cosmic rays, the formed secondary particles, and their energy, ^{7}Be and ^{10}Be production rates reach their maxima in the lower stratosphere (Poluianov et al., 2016). About two-thirds of ^{7}Be and ^{10}Be is produced in the stratosphere while the rest is

55   produced in the troposphere (Poluianov et al., 2016). Once produced, ^{7}Be and ^{10}Be rapidly attach to aerosol particles and get transported and deposited with their carrier aerosol by wet and dry deposition (Heikkilä et al., 2011). ^{10}Be has a half-life of 1.39 million years (Chmeleff et al., 2010) and its decay is thus negligible compared to atmospheric residence times. During transport away from the regions of their production, the ^{10}Be/^{7}Be ratio increases because ^{7}Be decays. The ratio ^{10}Be/^{7}Be therefore could indicate the path-integrated age of the air mass.

60   Due to different aerosol residence times in the stratosphere (more than 1 year) and troposphere (~weeks), the ^{10}Be/^{7}Be ratio is higher in the stratosphere than in the troposphere. Hence the ^{10}Be/^{7}Be ratio can be used to detect the stratosphere-troposphere exchange.

Many studies have focused on understanding the signals in surface ^{7}Be measurements from worldwide monitoring stations (Hernandez-Ceballos et al., 2015; Rodriguez-Perulero et al., 2019; Uhlar et al., 2020; Ajtić et

65   al., 2021; Burakowska et al., 2021). Due to the cosmogenic origin of ^{7}Be, surface air ^{7}Be concentrations are found to be connected to the 11-year cycle of solar modulation (Leppänen et al., 2010; Zheng et al., 2021a). In addition, ^{7}Be concentrations in the surface air are affected by different meteorological processes depending on locations, such as stratospheric intrusions (Jordan et al., 2003; Pacini et al., 2015; Yamagata et al., 2019), scavenging by precipitation (Chae and Kim, 2019; Kusmierczyk-Michulec et al., 2015), and vertical transport in the troposphere

70   (Aldahan et al., 2001; Ajtic et al., 2018; Zheng et al., 2021a).

The ability of general circulation models (e.g., ECHAM-HAM and GISS ModelE) and chemical transport models (e.g., GEOS-Chem) to capture the main characteristics in ^{7}Be and ^{10}Be transport and deposition has been shown by previous studies (e.g., Heikkilä et al., 2008b; Koch and Rind, 1998; Field et al., 2006; Usoskin et al., 2009; Brattich et al., 2021). For example, Usoskin et al. (2009) found that the solar proton-induced ^{7}Be production

75   peak in 2005 is indistinguishable from unforced variability given the amount of intrinsic variability through the comparison of GISS ModelE simulations and surface air measurements. By comparing the measurements with GEOS-Chem simulations, Brattich et al. (2021) found that increased ^{7}Be values in surface air samples in Northern Europe in early 2003 are associated with the instability of the Arctic polar vortex. In comparison to other

atmospheric models (e.g., Golubenko et al., 2021; Heikkilä et al., 2008b), the GEOS-Chem model is typically

80 driven by the GEOS assimilated data (e.g., MERRA-2 reanalysis data; Gelaro et al., 2017) that are closer to the meteorological observations than free-running general circulation model simulations. Further, GEOS-Chem can be run in a fine vertical resolution (72 levels), which is considered an important condition for realistic [7]Be and [10]Be tracer simulations (Heikkilä and Smith, 2012).

However, the default [7]Be production rate in the GEOS-Chem model is based on the outdated LP67

85 production rate which is based on observations made during the solar maximum year of 1958 (Liu et al., 2001). In comparison, the latest production models apply full Monte-Carlo simulations of the cosmic-ray-induced atmospheric nucleonic cascade (e.g., Poluianov et al., 2016; Masarik and Beer, 1999). LP67 shows the highest absolute [7]Be and [10]Be production rates compared to other production models (Elsässer, 2013). P16 suggests that LP67 overestimates the [7]Be production by 30-50% compared to their production model (Poluianov et al., 2016).

90 Furthermore, the LP67 production rates implemented in GEOS-Chem is only validated for the year 1958, a year with a high solar modulation (i.e., high solar activity) of 1200 MeV (Herbst et al., 2017). This highlights the problem of quantitatively comparing these uncorrected model outputs with measurements from other time periods. Certain modifications of solar modulation need to be applied in simulations for different years to account for changes in solar modulation. Previously, the production of [10]Be in GEOS-Chem was simply scaled

95 to the [7]Be production based on the ratio estimated from the surface measurements (Koch and Rind, 1998). In addition, [10]Be as simulated by GEOS-Chem has not been evaluated so far. It is hence necessary to update the beryllium production rates in GEOS-Chem and assess the corresponding impacts on model simulation results.

In this study, we incorporate global [7]Be and [10]Be production rates from recently published "CRAC:Be" (Cosmic Ray Atmospheric Cascade: Beryllium) model by Poluianov et al. (2016) into the GEOS-Chem model.

100 We simulate [7]Be and [10]Be using the GEOS-Chem with three different [7]Be and [10]Be production scenarios: GEOS-Chem default production using an empirical proximation (LP67 production), and two production scenarios derived from the "CRAC:Be" model with one considering realistic geomagnetic cut-off rigidity and the other considering only the dipole-moment of the geomagnetic field and an approximation of the resulting latitudinal variations in the cut-off rigidity (the so-called "Stoermer" cut-off).

105 This paper is organized as follows. Section 2 introduces the GEOS-Chem model and three different [7]Be and [10]Be production rates, discusses the methodology and experiment design, and describes the observational data for model evaluations. In section 3, we first investigate the differences between three different production scenarios (section 3.1). Then, we evaluate model simulations of [7]Be and [10]Be with several published datasets of [7]Be and [10]Be measurements, in terms of absolute values (section 3.2-3.3), vertical profiles (section 3.4), and seasonal variations

110 (section 3.5). The budgets and residence times of [7]Be and [10]Be are given in section 3.6. We also examine the [10]Be/[7]Be ratio in the model to assess its ability in capturing the stratosphere-troposphere exchange (section 3.7). Finally, we investigate the influence of including solar-induced production rate variability on [7]Be simulations (section 3.8). Summary and conclusions are given in section 4.

2 Models and Data

2.1 GEOS-Chem model

GEOS-Chem is global 3-D chemical transport model (http://www.geos-chem.org) with a detailed description of stratospheric and tropospheric chemistry coupled through the Unified tropospheric-stratospheric Chemistry Extension (Eastham et al., 2014; Bey et al., 2001). It is driven by archived meteorological data. We use version 14.0.2 (https://wiki.seas.harvard.edu/geos-chem/index.php/GEOS-Chem_14.0.2) to simulate the transport and deposition of atmospheric ^{7}Be and ^{10}Be. The standard model includes a radionuclide simulation option (^{222}Rn-^{210}Pb-^{7}Be-^{10}Be), which simulates transport (advection, convection, boundary layer mixing), deposition, and decay of the radionuclide tracers (e.g., Liu et al., 2001; Liu et al., 2004; Zhang et al., 2021a). It assumes that ^{7}Be and ^{10}Be are carried by ambient submicron aerosols after production and are removed by dry and wet deposition processes (Liu et al., 2001). The deposition scheme includes rainout (in-cloud scavenging) due to stratiform precipitation (Liu et al., 2001), scavenging in convective updrafts (Mari et al., 2000), and washout (below-cloud scavenging) by precipitation (Wang et al., 2011). Dry deposition is computed using the resistance-in-series scheme of Wang et al. (2011). Precipitation formation and evaporation fields from reanalysis data are used directly by the model wet deposition scheme.

In this work we drive GEOS-Chem with the Modern-Era Retrospective analysis for Research and Applications, Version 2 (MERRA-2) meteorological reanalysis dataset (http://gmao.gsfc.nasa.gov/reanalysis/MERRA-2/). MERRA-2 is a product of the Goddard Earth Observing System (GEOS) atmospheric data assimilation system, which assimilates modern observations of the atmosphere, ocean, land, and chemistry data (Gelaro et al., 2017). MERRA-2 has an original latitudinal resolution of 0.5° latitude by 0.667° longitude, with 72 vertical layers up to 0.01 hPa (80km). Here the MERRA-2 data are re-gridded to 4° latitude by 5° longitude for input to GEOS-Chem for computational efficiency.

2.2 ^{7}Be and ^{10}Be production models

The GEOS-Chem currently use the LP67 production rates of ^{7}Be and ^{10}Be (Lal and Peters, 1967). These production rates are calculated using an analytically estimated rate of nuclear "stars" in the atmosphere (stars/g air/s), multiplied with the mean production yield of 0.045 atoms/star for ^{7}Be and 0.025 atoms/star for ^{10}Be. These rates are represented as a function of latitude and altitude for the year 1958 and are not time-varying.

Here we update the atmospheric ^{7}Be and ^{10}Be production rates in GEOS-Chem with the latest production model: CRAC:Be model by P16 (Poluianov et al., 2016) using the solar modulation record by Herbst et al. (2017). The solar modulation record is based on the local interstellar spectrum by Herbst et al. (2017), which was also used in the production model. Given spatially and temporally resolved geomagnetic cut-off rigidities, the P16 model allows the calculation of 3-dimensional, temporally variable ^{7}Be and ^{10}Be production rates, which are necessary for input to atmospheric transport models. The P16 production model is regarded as the latest and most accurate production model for ^{7}Be and ^{10}Be and was used in recent general circulation model simulations (e.g., Golubenko et al., 2021; Sukhodolov et al., 2017).

The production of ^{7}Be and ^{10}Be is calculated by an integral of the yield function of ^{7}Be and ^{10}Be (Y_i, atoms g^{-1} cm^2 sr), and the energy spectrum of cosmic rays (J_i, (sr sec cm^2)$^{-1}$) above the cutoff energy E_c:

$$Q(\Phi, h, P_c) = \sum_i \int_{E_c}^{\infty} Y_i(E, h) J_i(E, \Phi) \, dE$$

The i refers to different types of primary cosmic ray particles (e.g., protons and alpha particles). The yield function Y_i is a function of height (h) and kinetic energy per incoming primary nucleon (E) and is directly taken from P16. The energy spectrum of cosmic rays J_i is a function of the cutoff energy (E_c) and the solar modulation (Φ), and is taken from Herbst et al. (2017). E_c is calculated as a function of the local geomagnetic rigidity cutoff (P_c):

$$E_c = E_r \left(\sqrt{1 + \left(\frac{Z_i \, P_c}{A_i E_r}\right)^2} - 1 \right)$$

where Z_i and A_i are the charge and mass numbers of particles, respectively. E_r is the rest mass of a proton (0.938 GeV).

The geomagnetic rigidity cutoff P_c is a quantitative estimation of the Earth's geomagnetic field shielding effect (Smart and Shea, 2005). Cosmic ray particles with rigidity (momentum per unit charge of the particle) higher than the geomagnetic cutoff rigidity value can enter the Earth's atmosphere. In most model simulations of ^{7}Be and ^{10}Be (e.g., Heikkilä et al., 2008c; Field et al., 2006; Koch et al., 1996; Liu et al., 2001), the production is calculated with a P_c simplified as a function of the geomagnetic latitude and geomagnetic dipole moment, called the vertical Stoermer cut-off rigidity equation (see equation 5.8.2-2 in Beer et al., 2012). However, this is different from the real geomagnetic cut-off rigidity inferred from the trajectories of particles with different energies using real geomagnetic field measurements (e.g., Copeland, 2018) which also includes non-dipole moments of the field (Beer et al., 2012) (Fig. S1).

Here we take the geomagnetic cutoff rigidity from Copeland (2018) that provides the cut-off rigidity at a fine interval (one degree) in both latitude and longitude. This production rate is denoted as P16$_{spa}$. To investigate the effect of this more realistic representation of cut-off rigidity on ^{7}Be and ^{10}Be simulations, we also perform simulations where the cut-off rigidities are approximated by the Stoermer equation (denoted as P16). The influence of the geomagnetic field intensity variations can be considered negligible on annual and decadal timescales and are ignored here (e.g. Muscheler et al., 2007; Zheng et al., 2020). It should be mentioned that the LP67 production is based on an ideal axial dipole cut-off rigidity similar to the P16 production model.

2.3 GEOS-Chem model experiments and evaluation

An overview of the performed simulations is shown in Table S1. The simulations are done using the P16spa and LP67 production rates from 2012 to 2018 with a four-year spinup (2008-2011). The average solar modulation is about 585 MeV for the period of 2012-2018. The default LP67 production rate used in GEOS-Chem is only for the year 1958 (with solar modulation of about 1200 MeV) and does not include the influences of the solar variations (e.g., 11-year solar cycle). However, it is difficult to correct such solar modulation influence for the model run since the varying solar modulation is latitudinally and vertically dependent. Hence, we do not apply any adjustments for the simulation with the LP67 production but bear in mind that it should, in principle,

underestimate production rates for the period of 2012-2018. A third simulation using the P16 production is also conducted for the year 2012 to evaluate the influence of production without considering the real geomagnetic cut-off rigidity. All simulations are done on a 4° latitude × 5° longitude resolution for computational efficiency (e.g., Liu et al., 2016; Liu et al., 2004).

190   To evaluate the model's ability to reproduce the variabilities in the observations, we use the statistical parameters: Spearman correlation coefficients and Root Mean Square Error (RMSE) (Chang and Hanna, 2004). Spearman rank correlation (R) (Myers et al., 2013) is used as it does not make any assumptions about the variables being normally distributed. It is less sensitive to abnormal values in the data compared to the commonly used Pearson correlation coefficients. The fraction of modeled concentrations within a factor of 2 of observations

195   (FA2) is calculated, i.e., for which $1/2 < x_{obs}/x_{mod} < 2$. Usually, if the scatter plot of the model and measurements is within a factor of 2 of observations, we consider the model with reasonably good performance.

2.4 [7]Be and [10]Be observational data for model validation

The annual mean [7]Be surface air concentration and deposition measurements are taken from a compilation by

200   Zhang et al. (2021b). The compilation includes a total of 494 annual mean values for surface air [7]Be concentrations and 304 for [7]Be deposition fluxes. For the deposition measurements, most of them include both wet and dry deposition, while a few are collected only during rainfall events and thus include only wet deposition. It includes the data from: a) the Environmental Measurements Laboratory (EML, https://www.wipp.energy.gov/namp/emllegacy/index.htm) Surface Air Sampling Program (SASP), which began

205   in the 1980s, b) the ongoing international monitor program Radioactivity Environmental Monitoring (REM) network (e.g., Hernandez-Ceballos et al., 2015; Sangiorgi et al., 2019), c) International Monitoring System (IMS) organized by the Comprehensive Nuclear-Test-Ban Treaty Organization (CTBTO) (e.g., Terzi and Kalinowski, 2017), and d) some additional datasets in publications not included in the above programs. This compiled [7]Be dataset only includes those data covering more than 1 year to reduce the influence of inherent seasonal variations.

210   We further include several recently published data for [7]Be surface air concentrations and deposition fluxes records that cover more than 1 year (Burakowska et al., 2021; Liu et al., 2022b; Kong et al., 2022).

      The dataset used for investigating the seasonality of [7]Be surface air concentrations are mainly taken from a multiyear compilation dataset of IMS from Terzi and Kalinowski (2017). The seasonal [7]Be deposition data are taken from Courtier et al. (2017), Du et al. (2015), Dueñas et al. (2017), Hu et al. (2020), Lee et al. (2015), and

215   Sangiorgi et al. (2019). The vertical profile of [7]Be concentrations is taken from the Environmental Measurements Laboratory (EML) High Altitude Sampling Program (HASP) spanning the years of 1962-1983. It should be noted, different from surface air measurements, the vertical air samples were usually collected during single-day flight campaigns.

      There are rather fewer [10]Be measurements compared to [7]Be. Here we compiled two datasets of published

220   [10]Be surface air measurements (Table S2) (Aldahan et al., 2008; Liu et al., 2022a; Yamagata et al., 2019; Padilla et al., 2019; Rodriguez-Perulero et al., 2019; Huang et al., 2010; Méndez-García et al., 2022; Elsässer et al., 2011; Dibb et al., 1994) and deposition fluxes (Table S3) covering more than 1 year, to validate the model performance. The deposition data include the precipitation samples (wet deposition) (Graham et al., 2003; Monaghan et al., 1986; Somayajulu et al., 1984; Heikkilä et al., 2008a; Raisbeck et al., 1979; Maejima et al., 2005) and ice core

samples (wet and dry deposition) that cover the recent period (Heikkilä et al., 2008a; Zheng et al., 2021b; Pedro et al., 2012; Baroni et al., 2011; Aldahan et al., 1998; Berggren et al., 2009; Auer et al., 2009). The ^{10}Be vertical profile measurements are mainly taken from Dibb et al. (1994, 1992) and Jordan et al. (2003).

3 Results and Discussions

3.1 ^{7}Be and ^{10}Be production

Figure 1 shows the comparison between the ^{7}Be production rates from the LP67 and P16 models for the years 1958 and 2012. Generally, the P16 production model shows a similar production distribution as the LP67 production rate, with a maximum ^{7}Be production over the polar stratosphere (~100 hPa). Compared to P16, the LP67 production rate shows differences up to 100%-160% higher values over the tropical stratosphere and 40-100% over the polar stratosphere (Fig. 1d). The LP67 production rate shows about 81% higher production rate compared to P16 in the stratosphere and 62% in the troposphere (Table S4). On a global average, the LP67 production rate is about 67% higher than that of P16. The stratospheric production rate contributes about 67% to the total production rate for LP67 while it is about 62% for the P16 production rate for the year 1958.
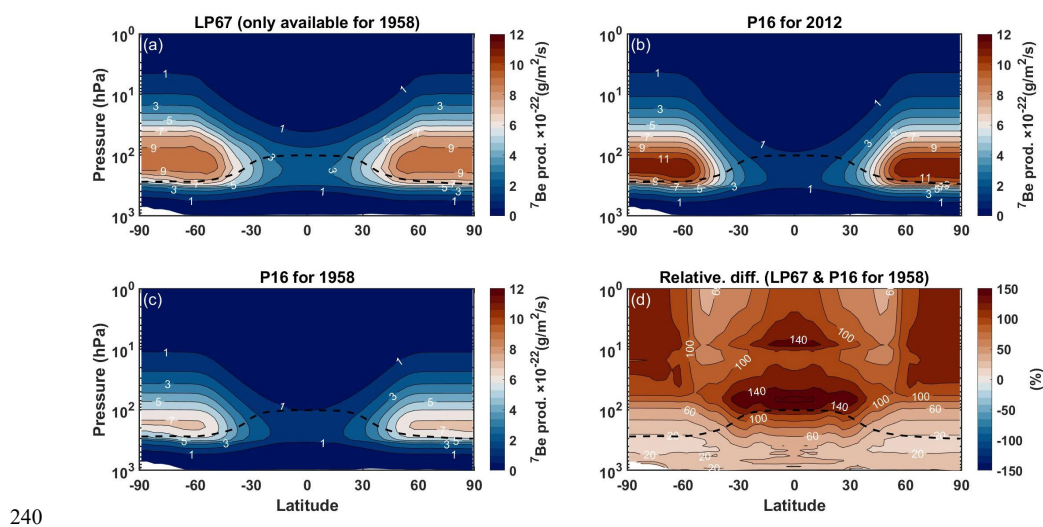
Figure 1. ^{7}Be production rates of (a) LP67 for the year 1958, (b) P16 for the year 2012, (c) P16 for the year 1958, and (d) relative differences (%) between LP67 and P16 production rates for the year 1958, i.e., (^{7}Be$_{LP67}$-^{7}Be$_{P16}$)/ ^{7}Be$_{P16}$×100%. The dashed line indicates the location of MERRA-2 thermal tropopause.

The ^{10}Be$_{LP67}$ production rate in the GEOS-Chem model uses the identical source distribution as ^{7}Be with a scaling factor based on the estimates from surface air measurements (Koch and Rind, 1998). This leads to a constant ^{10}Be$_{LP67}$/^{7}Be$_{LP67}$ production ratio (0.55) throughout the entire atmosphere. However, as shown in many ^{7}Be and ^{10}Be production models (e.g., Poluianov et al., 2016; Masarik and Beer, 2009), ^{7}Be and ^{10}Be have different altitudinal production distributions. The P16 production shows an increasing ^{10}Be/^{7}Be production ratio

250   from higher altitude (0.35) to lower altitude (0.6) (Fig. S2). Using a constant $^{10}Be/^{7}Be$ production ratio may thus result in large errors in the modelled ^{10}Be concentrations as well as $^{10}Be/^{7}Be$ ratios. The stratospheric production of ^{10}Be contributes about 67% of the total production with LP67 while it is about 58% with the P16 production for the year 1958 (Table S4).

    Figure 2 shows the comparison between $^{7}Be_{P16}$ and $^{7}Be_{P16spa}$ production rates for the year 2012. The global

255   production is similar for P16spa and P16 (Table S4). However, considering non-dipole moment influence on geomagnetic cut-off rigidity, $^{7}Be_{P16spa}$ and $^{10}Be_{P16spa}$ production rates in the Southern Hemisphere show ~11% higher production rates compared to the Northern Hemisphere (Table S4). This difference is not present when an axial dipole is assumed. Compared to P16 production rate, the $^{7}Be_{P16spa}$ production rates shows 40-50% lower production over eastern Asia and southeastern Pacific, but 20-30% higher over North America and from

260   subtropical South Atlantic to Australia (Fig. 2). $^{10}Be_{P16spa}$ (not shown) shows similar results but with less variability (e.g., 30-38% lower production rate over eastern Asia and subtropical South Atlantic relative to $^{10}Be_{P16}$). These differences are not constant throughout the atmospheric column but generally increase with altitude (Fig. 2).
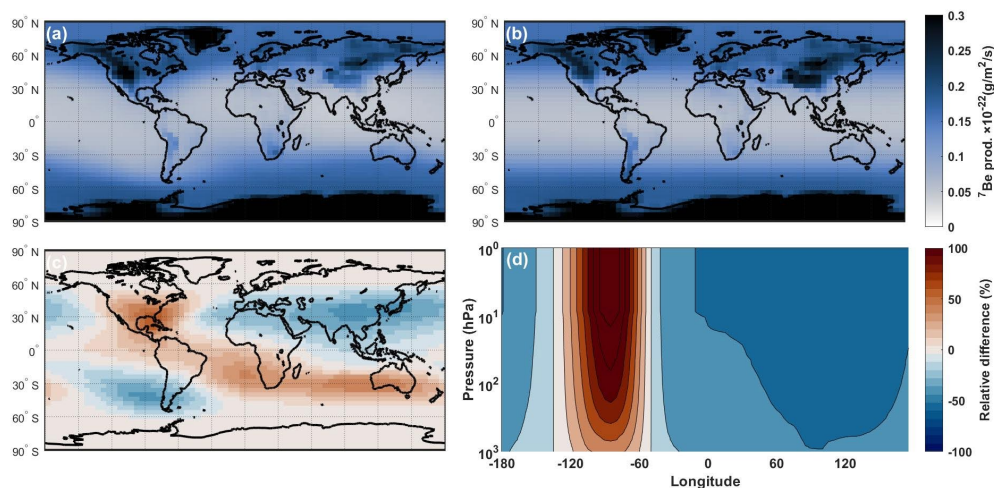
265   **Figure 2**. Upper panels: Spatial distribution of (a) P16spa and (b) P16 ^{7}Be production rates at 825 hPa. Lower panels: (c) Relative differences, i.e., $(^{7}Be_{P16spa}-^{7}Be_{P16})/^{7}Be_{P16} \times 100\%$, between production rates with and without considering the detailed spatial cut-off rigidity. (d) Relative differences of the zonal mean production rates between P16spa and P16 at 30°N.

3.2 ^{7}Be surface air concentrations and deposition fluxes

270   Figure 3 compares the simulated $^{7}Be_{P16spa}$ averaged over 2012-2018 with the measurements. Due to the data availability, the measurements do not necessarily cover the same period as model simulations. The model deposition fluxes here include both dry and wet deposition. About 94% of modeled air $^{7}Be_{P16spa}$ concentrations agree within a factor of 2 with the observed values. The model also shows reasonable agreement with the measured deposition fluxes (67% within a factor of 2) although the discrepancy between the modeled and

275   observed deposition fluxes is larger than that for surface air concentrations. The deposition fluxes are usually less well monitored compared to the air ^{7}Be samples and cover usually only shorter periods (e.g., one or two years).

Further, the limited model resolution applied here may not be able to capture local weather conditions (e.g., precipitation) in some sites, especially for coastal regions when the sub-grid scale orographic precipitation is important.
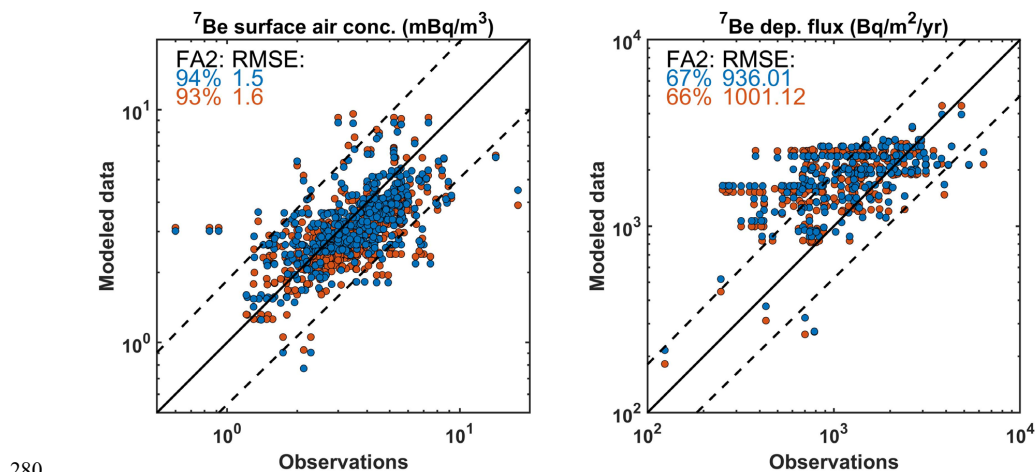
Figure 3. Scatter plot of modeled versus observed ^{7}Be surface air concentrations (left panel) and deposition fluxes (right panel). The model data is averaged over the years of 2012-2018. The dashed lines are the factor of 2 of 1:1 line (straight lines). Blue and orange colors indicate the model results using the P16spa and LP67 production rates, respectively. FA2 and RMSE for the two model simulations are also indicated. See text for details.

Figure 4 shows the spatial distribution and zonal mean of measurements in comparison with the model simulated ^{7}Be$_{P16spa}$ surface air concentrations and deposition fluxes. Generally, the model captures the spatial distribution of ^{7}Be air concentrations and deposition fluxes. The "latitudinal pattern" of surface air ^{7}Be concentrations differs from that of ^{7}Be production rates, reflecting the effects of atmospheric transport and deposition processes. The model suggests high ^{7}Be air concentrations mainly over the dry regions (Fig. 4a) due to low wet deposition rates (e.g., desert regions over Northern Africa, Arabian Peninsula, central Australia, and Antarctica) and over high-altitude regions (e.g., Tibetan Plateau). The model captures the observed latitudinal peaks in surface air concentrations over the subtropics and mid-latitudes (Fig. 4c around 30°N-40°N and 30°S -40°S). These peaks are consistent with the high stratospheric contribution (~25-30%) at mid-latitudes (Fig. S3). The model overestimates ^{7}Be air concentrations over the Arctic (70°N -90°N, Fig. 4c) by about 10%-20%. By contrast, high ^{7}Be deposition fluxes are observed at mid-latitudes due to the influence of the high precipitation (wet deposition) and strong stratosphere-troposphere exchange (Fig. 4d). In the Northern Hemisphere, the model simulated deposition fluxes peak at a lower latitude (~30°N) relative to the observations (~45°N). These modeled spatial distributions of the air concentrations and deposition rates of ^{7}Be also agree generally well with previous model simulations (e.g., Heikkilä and Smith, 2012).
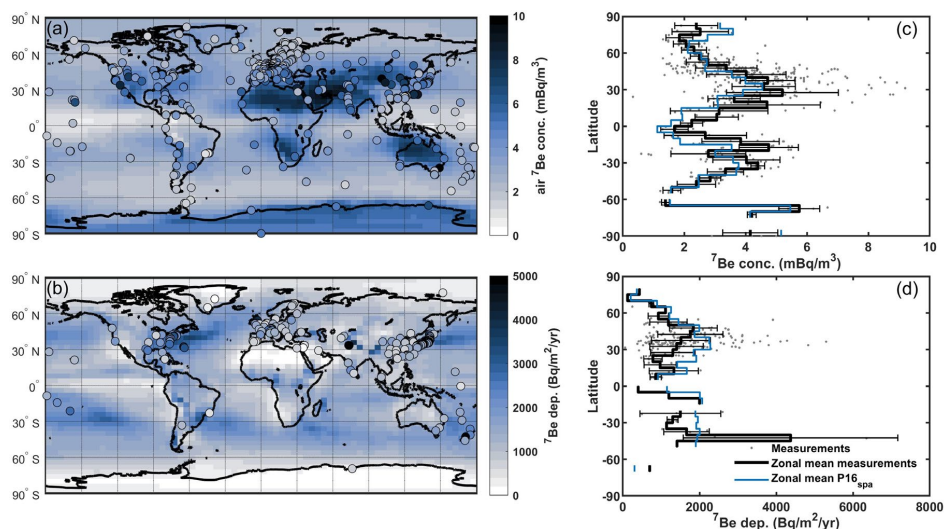
Figure 4. Left column: (a) modeled $^7Be_{P16spa}$ surface air concentrations (mBq/m^3) and (b) deposition fluxes (Bq/m^2/yr) averaged over the period 2012-2018. Color-coded dots denote ^7Be measurements. Right column: zonal mean of (c) observed ^7Be surface air concentrations and (d) deposition fluxes (black lines, for each 5° latitude bin) compared with the model simulation using the P16spa production rates (blue lines). Dots are individual measurements. The error bars indicate the standard error of the averages. The outliers, defined as more than three scaled median absolute deviations (MAD) away from the median, are excluded from the calculation.

Generally, the modeled $^7Be_{P16spa}$ air concentrations and deposition flux show slightly better agreement (smaller RMSE and higher FA2 values in Fig. 3) with the deposition measurements in comparison to $^7Be_{LP67}$. However, it should be kept in mind that LP67 is based on a too high solar modulation value of 1200 MeV instead of the 600 MeV which characterized the investigation period. Hence, LP67 should underestimate global mean production rates by 20-40%. Hence, this good agreement is caused by two compensating effects: i) the overestimation of ^7Be production for a given solar modulation and ii) a too high solar modulation value. Applying a scaling factor of 1.2-1.4 to account for the too high solar modulation leads to a larger RMSE compared to that with $^7Be_{P16spa}$ (upper panel of Fig. S4). For the $^7Be_{LP67}$ deposition fluxes, the scaling factor leads to an even larger disagreement between $^7Be_{LP67}$ and measurements (lower panel of Fig. S4).

We also examine whether using the dipole-approximation of the cut-off rigidity or real cut-off rigidity (P16 and P16spa, respectively) in the production model leads to significantly different results (Fig. 5). Although large differences in the production model are observed between P16spa and P16 production rates (up to 40-50% over eastern Asia and southern Pacific), such differences are reduced in surface air concentrations and deposition fluxes due to transport and deposition processes, as expected. The $^7Be_{P16sap}$ air concentrations show higher values (up to 7%) over 10°S -40°S and lower values (up to 13%) over the east Asian region (Fig. 5) compared to $^7Be_{P16}$. These differences are higher for the deposition fluxes with up to 10% over the 10°S-40°S and up to 20% over the east Asian region (Fig. 5). Since the total deposition flux reflects precipitation scavenging through the tropospheric column, it tends to be more sensitive to ^7Be air concentrations at higher altitudes and downward transport of ^7Be from the stratosphere. Indeed, model results suggest that deposition fluxes have a higher stratospheric fraction compared to the surface air concentrations (Fig. S3). The $^7Be_{P16spa}$ deposition fluxes show better agreement with measurements than those of $^7Be_{P16}$ (Fig. S5). The comparison for ^{10}Be shows similar results as ^7Be except with less than 10% differences. For ^{10}Be deposition fluxes in Antarctica and Greenland, this

330   influence is less than 3%. This is because the dominant contribution of [10]Be is from the stratosphere where the
hemispheric production differences are diminished by the long stratospheric residence time of [10]Be. However, it
does not suggest that the cut-off rigidity including the non-dipole influence could be ignored for [10]Be depositions
in polar regions, as the spatial pattern of cut-off rigidities was very different in the past time, e.g., during the
Laschamps geomagnetic field minimum around 41,000 years before the present (Gao et al., 2022). Further studies

335   are warranted to investigate this spatial cut-off rigidity influence on [10]Be in more detail.
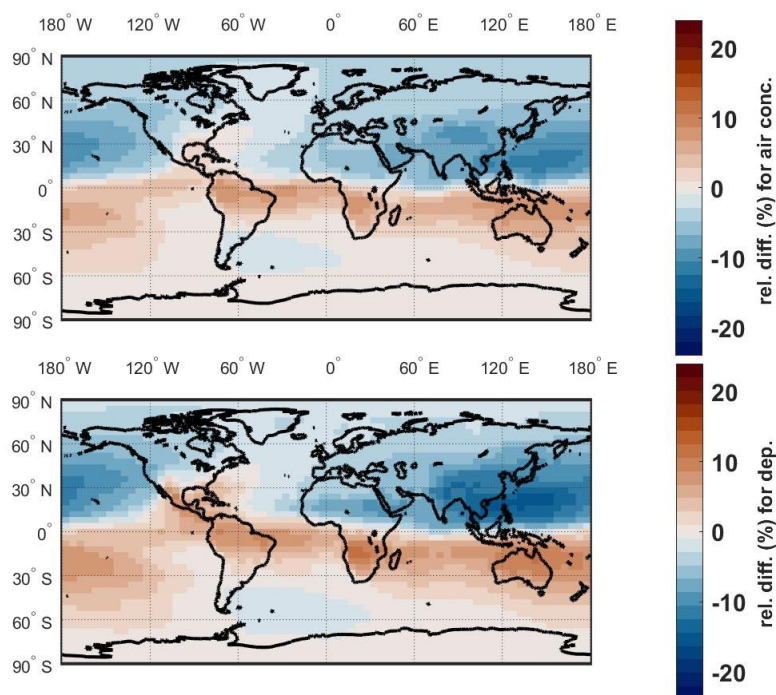
Figure 5. Relative differences (percentage) of surface air concentrations (upper panel) and deposition fluxes (lower panel) between [7]Be$_{P16spa}$ and [7]Be$_{P16}$ for the year 2012, i.e., ([7]Be$_{P16spa}$-[7]Be$_{P16}$)/ [7]Be$_{P16}$ ×100%.

340

3.3 [10]Be surface air concentrations and deposition fluxes

Figure 6 shows the comparison between modelled annual mean [10]Be$_{P16spa}$ surface air concentrations (or deposition
fluxes) averaged over 2012-2018 and measurements. The [10]Be$_{P16spa}$ shows similar spatial distributions as [7]Be$_{P16spa}$
because both radionuclides share the same transport and deposition processes. The model underestimates the

345   measured [10]Be surface air concentrations and deposition fluxes at some sites (Fig. 6b, 6d). This may be attributed
to the influence of resuspended dust with [10]Be attached, which could typically contribute 10%-35% to the air [10]Be
concentrations (Monaghan et al., 1986). It should be mentioned that [7]Be decays in the dust because of its short
half-life, and therefore does not contribute to the surface air [7]Be concentrations. Indeed, data where a careful
examination of the recycled dust [10]Be in samples was conducted (e.g., Monaghan et al., 1986), or from locations

350   that are less influenced by recycled dust [10]Be (e.g., Polar regions; dots in Fig. 6b-6d), show better agreement with the model simulations. This suggests the importance of considering the dust contribution when measuring the air [10]Be samples. The model also shows relatively good agreement with most [10]Be deposition data from polar ice cores (marked as dots in Fig. 6d) within a factor of 2. The [10]Be$_{P16spa}$ air and deposition results show smaller RMSE with "dust-free" samples (dots in Fig. 6) compared to [10]Be$_{LP67}$, suggesting better performance with the proper

355   simulation of [10]Be production. Furthermore, by considering the scaling factor for solar modulation correction for the LP67 production, even larger RMSE values between [10]Be$_{LP67}$ and the measurements are observed. The [10]Be$_{LP67}$ also shows a higher stratospheric fraction of surface air concentrations and deposition fluxes compared to [7]Be$_{P16spa}$ (Fig. S3).
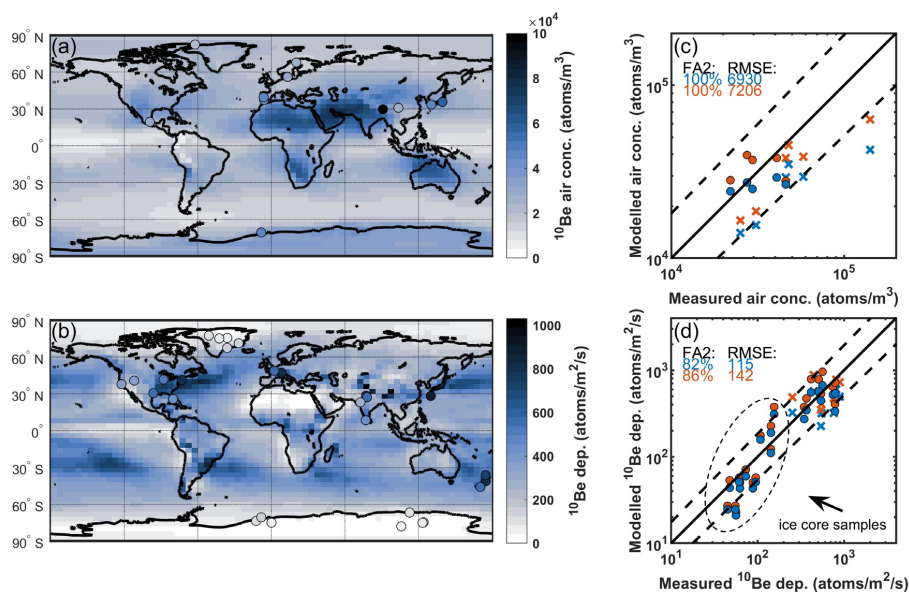
360

Figure 6. Left column: the modeled annual mean [10]Be$_{P16spa}$ (a) surface air concentrations and (b) deposition fluxes averaged over 2012-2018 overplotted with measurements (color-coded dots). Right column: (c)-(d) the scatter plot between model results and measurements for (c) surface air concentrations and (d) deposition fluxes. The dots in (c-d) indicate measurements with careful examination of dust [10]Be contributions or from the polar regions which are not influenced by dust [10]Be. The

365   crosses indicate the samples without examining dust contributions. The FA2 and RMSE are calculated only using the dust-free samples (dots). Blue and orange colors indicate the results using P16spa and LP67 production rates, respectively.

3.4 Vertical profiles of [7]Be and [10]Be

Figure 7 shows the simulated vertical profiles of [7]Be$_{P16spa}$ and [10]Be$_{P16spa}$ concentrations compared with those from

370   aircraft measurements in the troposphere and stratosphere. The measurements cover different regions and specific meteorological conditions; hence they should only provide a range in which the model results should lie. Following previous modelling studies (Heikkilä et al., 2008b; Koch et al., 1996), we compare model zonal mean values in each 15°latitude band with the corresponding observations.

375   The simulated $^{7}Be_{P16spa}$ profiles agree well with the measurements, especially capturing the peaks at ~20-22 km at mid- and low- latitudes (e.g., Fig. 7c, 7e, 7h). The increasing trend without a peak at northern high latitude (60°N-75°N) is also captured by the model (Fig. 7a). The $^{7}Be_{P16spa}$ shows high concentrations in the polar stratosphere and low values over the equatorial stratosphere (Fig. S6), mainly reflecting the latitudinal distribution of the production. This "latitudinal structure" is modulated for $^{10}Be_{P16spa}$ in the stratosphere as ^{10}Be is better mixed than ^{7}Be due to its slow decay together with relatively long residence time in the stratosphere (Waugh and Hall,

380   2002). Both ^{7}Be and ^{10}Be show very low concentrations in the tropical upper troposphere, reflecting the frequent injection of air from the lower troposphere in wet convective updrafts, where aerosols are efficiently scavenged (Fig. S6).
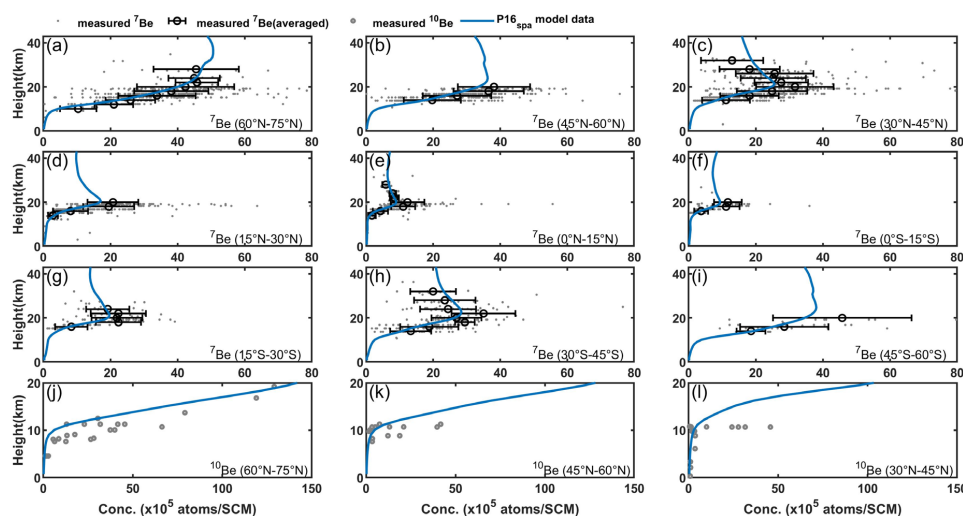
385   **Figure 7**. Comparison of the vertical profile between measurements (dots) and model zonal mean $^{7}Be_{p16spa}$ and $^{10}Be_{p16spa}$ concentrations for each latitudinal band (15°). The ^{7}Be (circle with error bar) observations are averaged for the altitude band of every 2 km where more than 5 samples are available. We also exclude the outlier from the calculation, which is defined as more than three scaled median absolute deviations (MAD) away from the median.

       The model also reasonably simulated ^{10}Be concentration vertical profiles compared with observations, with a

390   tendency to underestimate observations in the stratosphere (Fig. 7j-7l). A previous general circulation model study by also showed too low model stratospheric ^{10}Be compared to measurements. They attributed this underestimation to too short stratospheric air residence time in the model, which prevents ^{10}Be concentrations from accumulating sufficiently in the stratosphere. However, this may not be the case in our study, as the stratospheric air residence time in the MERRA-2 reanalysis agrees reasonably with the observations (Chabrillat et al., 2018). Another

395   explanation is that the ^{10}Be production rate may be underestimated in the stratosphere. ^{7}Be is less affected by this process than ^{10}Be because of its short half-life compared to its stratospheric residence time (Delaygue et al., 2015).

3.5 Global budgets and residence time

       Table 1 shows the global budgets for ^{7}Be and ^{10}Be over the period of 2012-2018. About 22.1% of tropospheric ^{7}Be

400   is lost by radioactive decay, 76.2% by convective and large-scale precipitation, and 1.7% by dry deposition. The wet deposition contributes to about 97% of total deposition in ^{7}Be and ^{10}Be, which is slightly higher than a 93%

contribution in previous model studies (Heikkilä et al., 2008b; Koch et al., 1996). The global mean tropospheric residence time of ^{7}Be is about 21 days, which is comparable to those reported by previous model studies: 18 days by Heikkilä et al. (2008b) and 21 days by Koch et al. (1996) and Liu et al. (2001). This also agrees with the

405   residence time of about 22-35 days estimated from the observed deposition fluxes and air concentrations at 30°N - 75°N (Bleichrodt, 1978). The averaged tropospheric residence time of ^{10}Be is about 24 days, which is consistent with the 20 days suggested by Heikkilä et al. (2008b). Interestingly, despite the fraction of ^{10}Be production in the stratosphere being higher for LP67 (67.5%) than P16spa (62.8%), the fraction of ^{10}Be stratospheric burden is similar for both: 94.3% for LP67 and 93.4% for P16spa. The latter is likely due to higher stratospheric production

410   in LP67 being compensated for more ^{10}Be being transported down to the troposphere.

Table 1. Global budgets of ^{7}Be and ^{10}Be averaged over the period 2012-2018 in GEOS-Chem using P16spa and LP67 production rates

	Simulation with P16spa		Simulation with LP67	
	^{7}Be	^{10}Be	^{7}Be	^{10}Be
Sources (g d^{-1})	0.366	0.231	0.402	0.320
Stratosphere	0.246 (67.21%)	0.145 (62.8%)	0.272 (67.7%)	0.216 (67.50%)
Troposphere	0.120 (32.79%)	0.086 (37.2%)	0.130 (32.3%)	0.104 (32.50%)
Sinks (g d^{-1})	0.365	0.231	0.403	0.316
Dry deposition	0.003 (0.82%)	0.006 (2.6%)	0.003 (0.7%)	0.008 (2.53%)
Wet deposition	0.138 (37.81%)	0.225 (97.4%)	0.140 (34.7%)	0.308 (97.47%)
Radioactive decay	0.224 (61.37%)	--	0.260 (64.5%)	--
Stratosphere	0.184 (50.41%)	--	0.217 (53.8%)	--
Troposphere	0.040 (10.96%)	--	0.043 (10.7%)	--
Burden (g)	17.236	84.140	19.972	142.929
Stratosphere	14.180 (82.27%)	78.552 (93.4%)	16.686 (83.5%)	134.768 (94.29%)
Troposphere	3.056 (17.73%)	5.588 (6.6%)	3.286 (16.5%)	8.100 (5.67%)
Tropospheric residence time (days)*	21.674	24.190	21.674	24.195

*against deposition only

415   **3.6 Seasonality in ^{7}Be and ^{10}Be**

The seasonality of ^{7}Be is influenced by a) the amount of precipitation; b) the stratosphere-troposphere exchange processes; and c) the vertical transport of ^{7}Be in the troposphere. The roles of these factors may vary depending on location. We compare the seasonal variations of modeled ^{7}Be$_{P16spa}$ and ^{7}Be$_{LP67}$ concentrations with measurements from a dataset compiled by Terzi and Kalinowski (2017) with the data covering more than 6 years (Fig. 8). It

420   should be noted that the model ^{7}Be results and MERRA-2 precipitation rates are averaged over the years of 2012-2018 while the measurements are based on the data availability during 2001-2015.
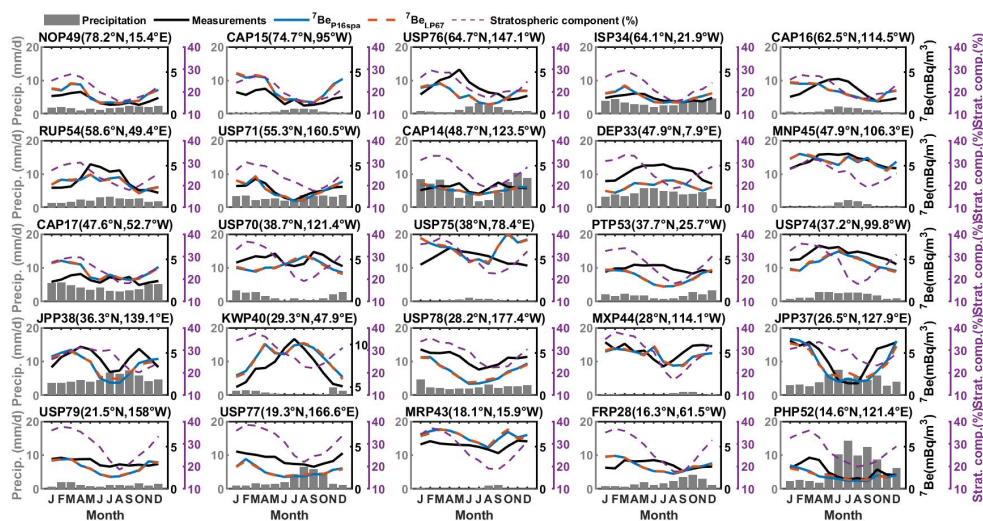
Figure 8. Seasonal cycle of simulated and measured surface air ^{7}Be concentrations, MERRA-2 total precipitation (4° x 5°, bar graph), and modeled stratospheric contributions to surface air. The plots are arranged based on the site latitudes. The model results using the LP67 production rates are normalized to the ones using the P16spa production rates.
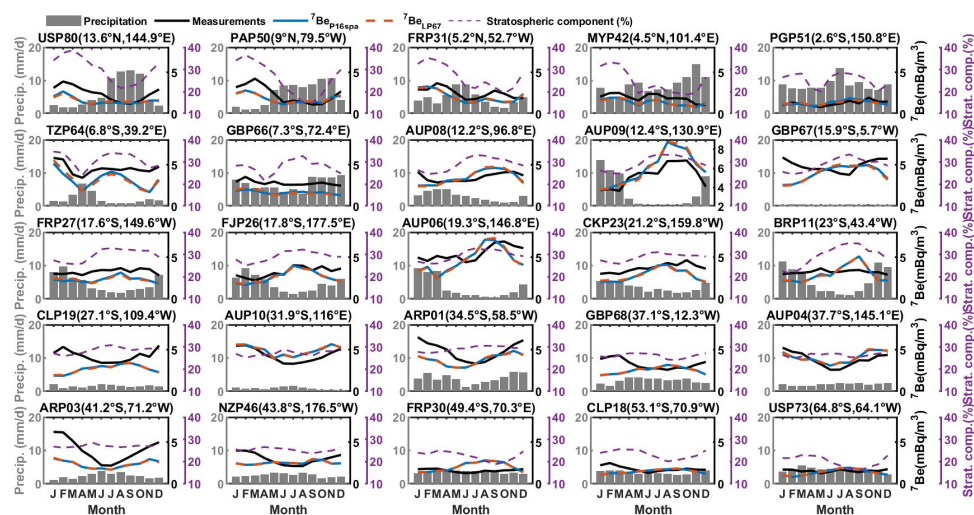
Figure 8. (continued)

In the Southern Hemisphere from 25°S-40°S, the ^{7}Be concentration peak is observed in austral summer (December-February), resulting from the combined influence of stratospheric intrusions and strong vertical transport during this season (Villarreal et al., 2022; Zheng et al., 2021a; Koch et al., 1996). The summer peak is also observed at northern mid-latitudes. This "summer peak" feature is well simulated by the model at some sites (e.g., KWP40(29.3°N, 47.9°E), AUP04(37.7°S, 145.1°E) and AUP10(31.9°S, 116°E) shown in Fig. 8) but not at others (e.g., GBP68(37.1°S, 12.3°W) and PTP53(37.7°N, 25.7°W) in Fig. 8). This may not be related to stratospheric intrusion in the model as the simulated stratospheric contributions (Fig. S3) agree fairly well with

estimates inferred from measurements, i.e., ~25% on annual average at northern mid-latitude surface (Dutkiewicz and Husain, 1985; Liu et al., 2016). Hence this could be due to the errors in vertical transport (e.g., convection) during the summer season.

The sites at northern high-latitudes (>50°N) show spring peaks that are well simulated by the model (e.g.,
440   ISP3(64.1°N, 21.9°W)). This spring peak coincides with high stratospheric contributions, reflecting the influence of stratospheric intrusions. The influence of precipitation changes is also seen at several sites, especially in locations with high precipitation rates (e.g., monsoon regions). For example, two sites from Japan (JPP38(36.3°N, 139.1°E) and JPP37(26.5°N, 127.9°E) in Fig. 8) show summer minima coinciding with the high precipitation, even with relatively high stratospheric contributions in the same month.

445   The seasonal variation of stratospheric contribution is quite similar for the sites located in the Northern Hemisphere, with a high contribution in spring and a low contribution in fall. This is consistent with the estimates based on air samples that indicate stratospheric contributions varying from ~40% in spring to ~15% in fall at latitudes 38°N-51°N (Dutkiewicz and Husain, 1985).

Generally, the model simulates well the annual cycle of surface air ^{7}Be concentrations for most sites in terms
450   of amplitude and seasonality (Fig.8). For a few sites (e.g., DEP33(47.9°N, 7.9°E)), the model captures the observed seasonality but not the correct absolute values. This could be partly due to the coarse resolution of the model. The ^{7}Be$_{LP67}$ is normalized to ^{7}Be$_{P16spa}$ as we focus on the comparison of seasonal variability between these simulations. The very similar features (differences within 1%) between all simulations using different production rates indicate a dominant influence of the meteorological conditions on the seasonal variations of the air ^{7}Be
455   concentrations.
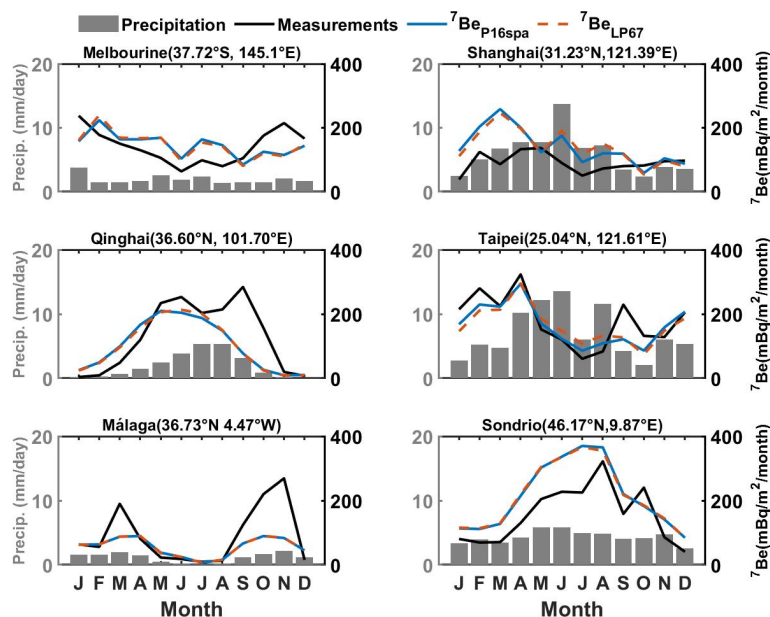
Figure 9. Seasonal cycle of simulated (color lines) and measured (black line) ^{7}Be deposition fluxes together with MERRA-2 total precipitation (4° x 5°, bar graph). The model results using the LP67 production rates are normalized to the ones using the P16spa production rates.

460   Figure 9 compares model results with the seasonal [7]Be deposition flux observations. Usually, high precipitation leads to high [7]Be deposition fluxes (e.g., Du et al., 2015). Interestingly, low deposition fluxes are observed during the summer season in Taipei (Lee et al., 2015; Huh et al., 2006) coinciding with high precipitation. This feature is well-captured in the model. Taipei has a typhoon season in summer when strong precipitation can occur in a very short period. The atmospheric [7]Be could be removed quickly at the early stage of

465   the precipitation event while at the later stage there is little [7]Be left in the air that can be removed (Ioannidou and Papastefanou, 2006). The feature of double peaks in Malaga is well captured by the model, although the amplitude of peaks is largely underestimated. This may be because of the coarse resolution of the model not capturing the orographic effects on local precipitation of the coastal mountain range.

To examine the model's ability to simulate [10]Be in polar regions, we compare model results with two

470   sub-annual ice cores records (Fig. 10): the GRIP record from Greenland (1986-1990) (Heikkilä et al., 2008c) and the DSS record from Antarctica (2000-2009) (Pedro et al., 2011a). It should be noted that the direct measurements from ice cores are concentrations in the ice (atoms/g). To calculate deposition fluxes, the ice concentrations are multiplied with ice accumulation rates. However, for sub-annual accumulations, this bears large uncertainties. Therefore, we calculate the modelled [10]Be concentrations for the selected sites using the model deposition fluxes

475   at the selected sites timed by ice density and then divided by the corresponding model precipitation rates.
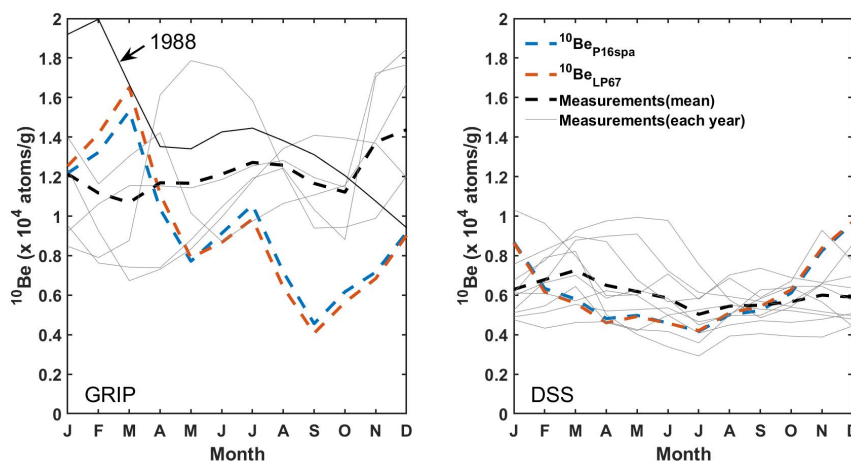
Figure 10. Seasonal cycle of simulated [10]Be deposition fluxes (2012-2018) and measured [10]Be deposition fluxes in GRIP (1986-1990) and DSS (2000-2009) ice cores. The solid lines (grey) refer to seasonal variations of the measurements for each year. The black solid line indicates seasonal data of measurements in the year 1988. The dashed lines indicate the averaged
480   seasonal variations of measured [10]Be (black), [10]Be$_{P16spa}$ (blue), and [10]Be$_{LP67}$ (red) concentrations.

Firstly, there is no consistent seasonal cycle in the GIRP [10]Be measurement, indicating a strong role of local meteorology. The model does not reproduce the mean seasonal cycle partly because the model was not run for the exact same period. However, we note that the measurements for the year 1988 show an annual cycle similar to that in the model, suggesting that the model [10]Be seasonality falls within the range of the observations. For the DSS

485   site, the model simulates the austral winter minima but not the austral fall maxima (February-April). These model biases could be due to the limited model resolution and local effects (e.g., ice redistribution due to wind blow) that are not resolved by the model. Such discrepancies were also reported by previous model studies using the ECHAM-HAM general circulation model over the overlap period (Heikkilä et al., 2008c; Pedro et al., 2011b). It

should be kept in mind that local surface processes cause a high degree of spatial variability in the impurity
490 concentrations in ice cores even on short distances (Gfeller et al., 2014), which cannot be captured in our model.

3.7 ^{10}Be/^{7}Be ratio

Figure 11 shows the modelled zonal mean ^{10}Be/^{7}Be ratios during boreal spring (March-May) and austral spring (September-November), respectively, when the stratosphere-troposphere exchange is strong in either of the two hemispheres. Also shown are the comparison of the altitudinal profile of the ^{10}Be/^{7}Be ratio with
495 measurements from three aircraft missions (Jordan et al., 2003). The model ^{10}Be/^{7}Be ratio generally lies within the ranges of measurements. Due to the decay of the ^{7}Be and long residence time in the stratosphere, the ^{10}Be/^{7}Be ratio is higher (>1.5) in the stratosphere and increase over the altitude, with a maximum (>10) in the tropical stratosphere. During the period without strong stratospheric intrusion (e.g., autumn season in the Northern Hemisphere, Fig.11b), the monthly ^{10}Be/^{7}Be ratio near the surface is around 0.9~1. This surface ^{10}Be/^{7}Be ratio
500 could be up to 1.4 when the strong stratosphere-troposphere exchange happens.
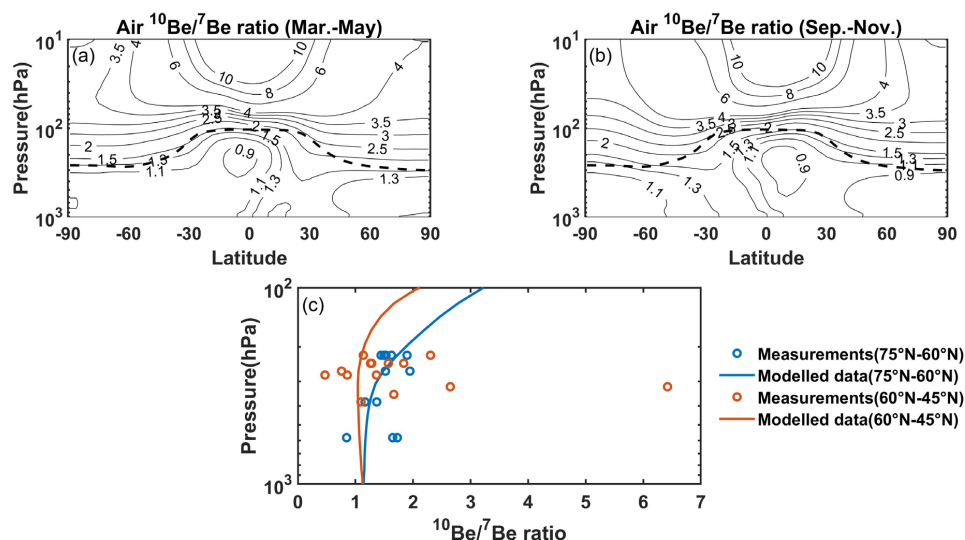
Figure 11. Upper panels: simulated ^{10}Be/^{7}Be ratio in spring (March-May) (a) and autumn (September-November) (b) averaged over the years 2012-2018. Lower panel (c): comparison between the annual averaged model ^{10}Be/^{7}Be ratios (lines) and those from measurements (circles; Jordan et al., 2003). The comparison is shown for the latitude bands of 75°N-60°N and
505 60°N-45°N, respectively.

Figure 12 compares model surface air ^{7}Be and ^{10}Be concentrations and ^{10}Be/^{7}Be ratios with monthly mean observations in Tokyo (Yamagata et al., 2019) during the period of 2012-2014. Here we mainly focus on the relative variations, and measured ^{7}Be and ^{10}Be data are normalized to the model values (i.e., divided by the measurement mean and multiplied by the model mean). The model captures the observed variability in Tokyo
510 well. The ^{7}Be and ^{10}Be show a peak in early spring (March-May) while the ^{10}Be/^{7}Be ratio shows a wider peak over March-July. The summer minima of ^{7}Be and ^{10}Be are due to strong scavenging associated with the monsoon/typhoon season precipitation. While the ^{10}Be/^{7}Be ratio is independent of precipitation scavenging, the peaks of ^{10}Be/^{7}Be coincide well with the enhancements of stratospheric contribution in the model. This indicates

that the ^{10}Be/^{7}Be ratio is a better indicator of the vertical transport and stratospheric intrusion influences than
515   either tracer alone.
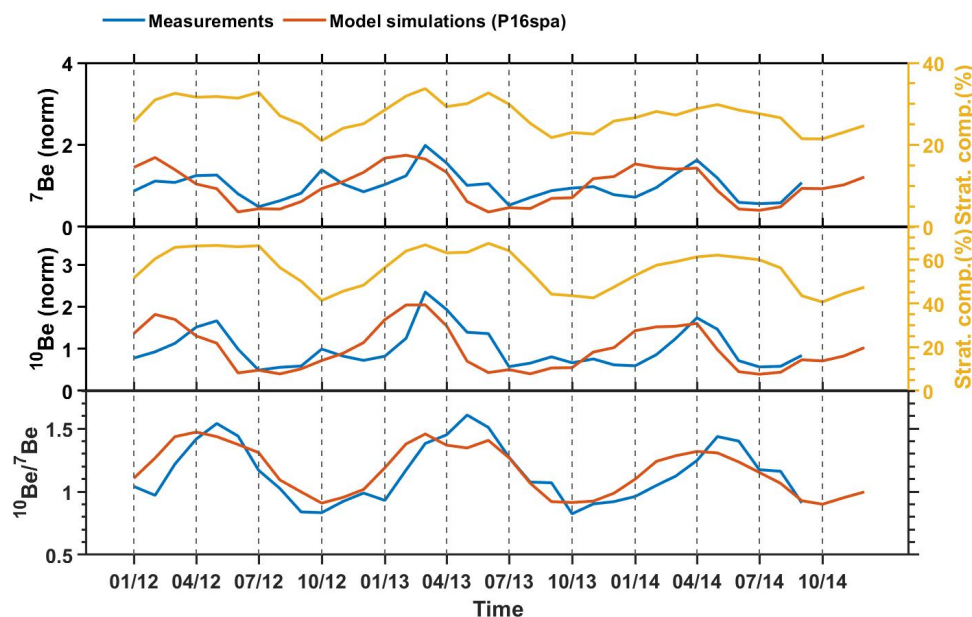
Figure 12. Comparison of monthly mean ^{7}Be (top panel), ^{10}Be (middle panel) concentrations, and ^{10}Be /^{7}Be ratio (bottom panel) between model results and measurements for the Tokyo station over the period 2012-2014. Noted that the measured ^{10}Be and ^{7}Be concentrations are normalized to model values (i.e., divided by the measurement mean and then multiplied by the
520   model mean) to focus on variability.

3.7 Solar modulation influences

Here we examine the model's ability to simulate the inter-annual variability of ^{7}Be surface air concentrations, especially whether the model can simulate the solar modulation influence using the updated production model. Figure 13 shows the comparison of model simulated annual mean surface air ^{7}Be concentrations with
525   measurements during 2012-2018 from four sites: Kiruna, Ljungbyhed, Vienna and Hong Kong (Kong et al., 2022; Zheng et al., 2021a). The tropospheric ^{7}Be production rate from each site is also plotted for comparison as measured annual mean surface air ^{7}Be concentrations are predominantly influenced by the local tropospheric ^{7}Be production signal (Zheng et al., 2021a). This is due to the relatively large variation (up to 25% deviation of the mean) of the ^{7}Be production rates associated with the 11-year solar cycle at high latitudes (Fig. 13).

530   The model ^{7}Be$_{P16spa}$ surface air concentrations show better agreement with annual ^{7}Be measurements (higher R-value) compared to ^{7}Be$_{LP67}$ concentrations at all surface sites, except for Hong Kong (Fig. 13). The interannual variation of surface air ^{7}Be concentration at Hong Kong mainly reflects the meteorological influences instead of the production (solar) signal. The increasing trend in the measurements (Kiruna, Ljungbyhed, and Vienna) after 2015 agrees well with the trend in production, suggesting a dominant influence of solar modulation during this
535   period. This is further supported by strong deviations between ^{7}Be$_{P16spa}$ and ^{7}Be$_{LP67}$ after 2015 as no solar influence is considered in ^{7}Be$_{LP67}$. This also emphasizes the importance of including solar modulation of the ^{7}Be and ^{10}Be production in modeling studies, especially for high-latitude regions. The mismatch of trends in

measurements and production from 2012 to 2015, together with the similar year-to-year variability between $^7Be_{P16spa}$ and $^7Be_{LP67}$, suggests the meteorological influence is dominant at those sites for this period. This also

540   suggests that meteorological influences can suppress the solar signal in the ^7Be and ^{10}Be observations.
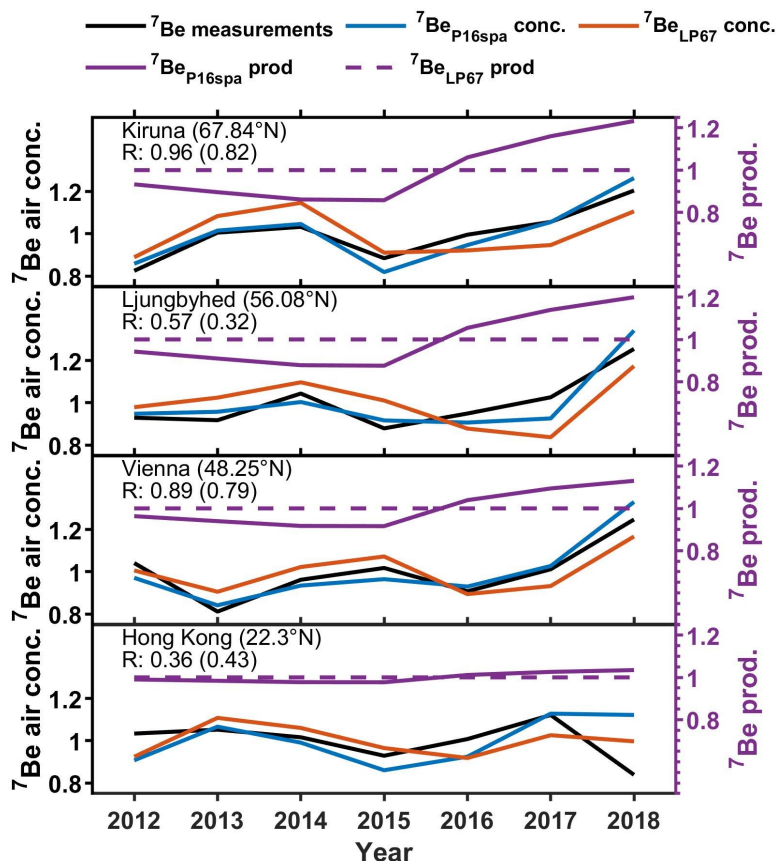
Figure 13. Comparison of annual mean model surface air ^7Be concentrations with measurements from 2012-2018. Also shown are the model tropospheric ^7Be production (purple lines) at each station. All data are normalized by being divided by the mean. The linear correlation coefficient R-value in the bracket is for the $^7Be_{LP67}$ simulation.

545   **4 Summary and conclusions**

We have incorporated the ^7Be and ^{10}Be production rates derived from the CRAC:Be model into the GEOS-Chem global chemical transport model, enabling the model output to be quantitively comparable with the measurements. We simulate ^7Be and ^{10}Be using GEOS-Chem with three different ^7Be and ^{10}Be production scenarios: default production rate in the model using an empirical proximation (LP67 production), and two production scenarios

550   derived from the CRAC:Be model with one considering realistic geomagnetic cut-off rigidity (P16$_{spa}$ production rate) and an ideal dipole cut-off rigidity (P16 production rate). On global average, the LP67 production rate is 67% higher compared to those of P16 and P16spa. On the other hand, the P16 production rate shows some regional differences (up to 50%) compared to the P16spa production rate.

In comparison with a large amount of air and deposition flux measurements, the model $^7Be_{P16spa}$ shows good
agreements with respect to surface air concentrations (94% of data within a factor of 2) and reasonably good
agreements regarding deposition fluxes (67% of data within a factor of 2). The model well simulates the surface
air concentration peaks in the subtropics associated strong downward transport from the stratosphere. This
agreement is better than those using the default production $^7Be_{LP16}$ and the $^7Be_{P16}$ production with simplified axis
symmetric dipole cut-off rigidity. The $^7Be_{LP67}$ simulation tends to overestimate the absolute value of ^7Be and ^{10}Be.
The $^7Be_{P16}$ simulation tends to produce a positive bias (~20%) for the ^7Be deposition fluxes in East Asia region,
nevertheless, no large bias is found for ^7Be surface air concentrations. The surface deposition fluxes are more
sensitive to the production in the mid- and upper-troposphere due to the effect of precipitation scavenging
throughout the troposphere.

For the first time, the ability of GEOS-Chem to simulate ^{10}Be is also assessed with measurements. The model
$^{10}Be_{P16spa}$ results agree well with ^{10}Be observational data that were evaluated for dust influences or from the
regions less influenced by dust (e.g., polar regions), while underestimating most samples that were not corrected
for dust influences. This highlights the importance of examining the dust contribution to ^{10}Be measurements when
using these data to evaluate models.

Independent of the production models, surface ^7Be and ^{10}Be concentrations from all three simulations show
similar seasonal variations, suggesting a dominant meteorological influence. The model generally simulates well
the annual cycle of ^7Be surface air concentrations and deposition fluxes at most sites in terms of amplitude and
seasonality. The model fails to capture the "summer peak" in a few sites likely due to errors in convective
transport during summer.

The model $^{10}Be/^7Be$ ratios also lie within the measurements, suggesting the stratosphere-troposphere
exchange process is reasonably represented in the model. The mismatch of the peaks between $^7Be(^{10}Be)$ and
$^{10}Be/^7Be$ ratios at the Tokyo site suggests that the $^{10}Be/^7Be$ ratio is a better indicator of the vertical transport and
stratospheric influences than either tracer alone as the ratio is independent of precipitation scavenging.

Finally, we demonstrate the value and importance of including time-varying solar modulation in ^7Be and
^{10}Be production rates for model simulations of both tracers. It significantly improves the agreement of interannual
variations between the model and measurements, especially at those surface sites from mid- and high- latitudes.
The mismatch of trends in modelled ^7Be production rates and observed air concentrations from 2012-2015 also
suggests that the solar signal can be suppressed by meteorological influences.

In summary, we have shown that with the state-of-the-art P16spa production rate, the ability of GEOS-Chem
to reproduce the ^7Be and ^{10}Be measurements (including interannual variability of ^7Be) is significantly improved.
While uncertainties in transport and deposition processes play a major role in the model performance, reduced
uncertainties in the production rates, as demonstrated in this study, allow us to use ^7Be and ^{10}Be tracers as better
tools for evaluating and testing transport and scavenging in global models.

Author contributions. MZ initiated the study. MZ performed the analysis and interpretation with contributions
from HL and FA. MZ conducted the GEOS-Chem model simulations with the help from MW. All authors
discussed the results and edited the manuscript.

Competing interests. The authors declare that there is no conflict of interest.

595

Data and Code availability. Observational data for model validation are available in the references described in section 2.3. The two compiled [10]Be observation datasets are available in the Supplementary Information. The GEOS-Chem v14.0.2 model code, GEOS-Chem model output and [7]Be and [10]Be production rates are available at Zenodo repository (https://doi.org/10.5281/zenodo.8051729; Zheng et al., 2023).

600

Acknowledgments. This project is supported by the Swedish Research Council (Dnr: 2021-06649) and the Swedish government funded Strategic Research Area: ModElling the Regional and Global Earth system, MERGE (MERGE). H. Liu acknowledges funding support from the NASA Modeling, Analysis and Prediction (MAP) program (grant 80NSSC17K0221) and Atmospheric Composition Campaign Data Analysis and Modeling program (grants NNX14AR07G and 80NSSC21K1455). F. Adolphi acknowledges support from the Helmholtz association (Grant number VH-NG 1501). R. Muscheler acknowledges support from the Swedish Research Council (grants DNR2013-8421 and DNR2018-05469). Z. Lu acknowledges Swedish Research Council Vetenskapsrådet (Grant No. 2022-03617). M. Wu acknowledges the National Natural Science Foundation of China (42111530184, 41901266). N. Prisle acknowledges the funding from the Academy of Finland (Grant Nos. 308238, 314175, and 335649). This project has received funding from the European Research Council (ERC) under the European Union's Horizon 2020 research and innovation programme, Project SURFACE (Grant Agreement No. 717022). The GEOS-Chem model is managed by the Atmospheric Chemistry Modeling Group at Harvard University. GEOS-Chem support team at Harvard University and Washington University in St. Louis (WashU) is acknowledged for their effort. GEOS-Chem input files were obtained from the GEOS-Chem Data Portal enabled by WashU.

References

Ajtic, J., Brattich, E., Sarvan, D., Djurdjevic, V., and Hernandez-Ceballos, M. A.: Factors affecting the [7]Be surface concentration and its extremely high occurrences over the Scandinavian Peninsula during autumn and winter, Chemosphere, 199, 278-285, 10.1016/j.chemosphere.2018.02.052, 2018.

Ajtić, J., Zorko, B., Nečemer, M., Sarvan, D., Rajačić, M., Krneta Nikolić, J., Todorović, D., Djurdjevic, V., Vodenik, B., Glavič Cindro, D., and Kožar Logar, J.: Characteristics of radioactivity in the surface air along the 45°N zonal belt in South-Eastern Europe, International Journal of Environmental Science and Technology, 10.1007/s13762-021-03814-0, 2021.

Aldahan, A., Possnert, G., and Vintersved, I.: Atmospheric interactions at northern high latitudes from weekly Be-isotopes in surface air, Applied Radiation and Isotopes, 54, 345-353, https://doi.org/10.1016/S0969-8043(00)00163-9, 2001.

Aldahan, A., Hedfors, J., Possnert, G., Kulan, A., Berggren, A. M., and Söderström, C.: Atmospheric impact on beryllium isotopes as solar activity proxy, Geophys Res Lett, 35, 10.1029/2008gl035189, 2008.

Aldahan, A., Possnert, G., Johnsen, S. J., Clausen, H. B., Isaksson, E., Karlen, W., and Hansson, M.: Sixty year [10]Be record from Greenland and Antarctica, Earth and Planetary Sciences, 107, 139-147, 10.1007/BF02840464, 1998.

635   Auer, M., Wagenbach, D., Wild, E. M., Wallner, A., Priller, A., Miller, H., Schlosser, C., and Kutschera, W.: Cosmogenic 26Al in the atmosphere and the prospect of a 26Al/10Be chronometer to date old ice, Earth and Planetary Science Letters, 287, 453-462, https://doi.org/10.1016/j.epsl.2009.08.030, 2009.

Baroni, M., Bard, E., Petit, J.-R., Magand, O., and Bourlès, D.: Volcanic and solar activity, and atmospheric circulation influences on cosmogenic [10]Be fallout at Vostok and Concordia (Antarctica) over the last 60 years, Geochimica et Cosmochimica Acta, 75, 7132-7145, 10.1016/j.gca.2011.09.002, 2011.

640   Beer, J., McCracken, K., and Von Steiger, R.: Cosmogenic Radionuclides: Theory and Applications in the Terrestrial and Space Environments, Springer Science & Business Media2012.

Berggren, A. M., Beer, J., Possnert, G., Aldahan, A., Kubik, P., Christl, M., Johnsen, S. J., Abreu, J., and Vinther, B. M.: A 600-year annual [10]Be record from the NGRIP ice core, Greenland, Geophys Res Lett, 36, L11801, 10.1029/2009gl038004, 2009.

645   Bleichrodt, J. F.: Mean tropospheric residence time of cosmic-ray-produced beryllium 7 at north temperate latitudes, Journal of Geophysical Research: Oceans, 83, 3058-3062, https://doi.org/10.1029/JC083iC06p03058, 1978.

Brattich, E., Liu, H., Zhang, B., Hernández-Ceballos, M. Á., Paatero, J., Sarvan, D., Djurdjevic, V., Tositti, L., and Ajtić, J.: Observation and modeling of high-7Be events in Northern Europe associated with the instability of

650   the Arctic polar vortex in early 2003, Atmos. Chem. Phys. Discuss., 2021, 1-43, 10.5194/acp-2020-1121, 2021.

Burakowska, A., Kubicki, M., Myslek-Laurikainen, B., Piotrowski, M., Trzaskowska, H., and Sosnowiec, R.: Concentration of (7)Be, (210)Pb, (40)K, (137)Cs, (134)Cs radionuclides in the ground layer of the atmosphere in the polar (Hornsund, Spitsbergen) and mid-latitudes (Otwock-Swider, Poland) regions, J Environ Radioact, 240, 106739, 10.1016/j.jenvrad.2021.106739, 2021.

655   Chabrillat, S., Vigouroux, C., Christophe, Y., Engel, A., Errera, Q., Minganti, D., Monge-Sanz, B. M., Segers, A., and Mahieu, E.: Comparison of mean age of air in five reanalyses using the BASCOE transport model, Atmospheric Chemistry and Physics, 18, 14715-14735, 10.5194/acp-18-14715-2018, 2018.

Chae, J.-S. and Kim, G.: Large seasonal variations in fine aerosol precipitation rates revealed using cosmogenic [7]Be as a tracer, Science of The Total Environment, 673, 1-6, https://doi.org/10.1016/j.scitotenv.2019.03.482,

660   2019.

Chang, J. C. and Hanna, S. R.: Air quality model performance evaluation, Meteorology and Atmospheric Physics, 87, 10.1007/s00703-003-0070-7, 2004.

Chmeleff, J., von Blanckenburg, F., Kossert, K., and Jakob, D.: Determination of the 10Be half-life by multicollector ICP-MS and liquid scintillation counting, Nuclear Instruments and Methods in Physics Research

665   Section B: Beam Interactions with Materials and Atoms, 268, 192-199, 10.1016/j.nimb.2009.09.012, 2010.

Copeland, K.: CARI-7 Documentation: Geomagnetic Cutoff Rigidity Calculations and Tables for 1965-2010, United States. Department of Transportation. Federal Aviation Administration …, 2018.

Courtier, J., Sdraulig, S., and Hirth, G.: 7Be and 210Pb wet/dry deposition in Melbourne, Australia and the development of deployable units for radiological emergency monitoring, Journal of Environmental

670   Radioactivity, 178-179, 419-425, https://doi.org/10.1016/j.jenvrad.2017.07.004, 2017.

Delaygue, G., Bekki, S., and Bard, E.: Modelling the stratospheric budget of beryllium isotopes, Tellus B: Chemical and Physical Meteorology, 67, 28582, 10.3402/tellusb.v67.28582, 2015.

Dibb, J. E., Talbot, R. W., and Gregory, G. L.: Beryllium 7 and Lead 210 in the western hemisphere Arctic atmosphere: Observations from three recent aircraft-based sampling programs, Journal of Geophysical Research: Atmospheres, 97, 16709-16715, 10.1029/91JD01807, 1992.

Dibb, J. E., Meeker, L. D., Finkel, R. C., Southon, J. R., Caffee, M. W., and Barrie, L. A.: Estimation of stratospheric input to the Arctic troposphere: [7]Be and [10]Be in aerosols at Alert, Canada, 99, 12855-12864, 10.1029/94jd00742, 1994.

Du, J., Du, J., Baskaran, M., Bi, Q., Huang, D., and Jiang, Y.: Temporal variations of atmospheric depositional fluxes of7Be and210Pb over 8 years (2006-2013) at Shanghai, China, and synthesis of global fallout data, Journal of Geophysical Research: Atmospheres, 120, 4323-4339, 10.1002/2014jd022807, 2015.

Dueñas, C., Gordo, E., Liger, E., Cabello, M., Cañete, S., Pérez, M., and Torre-Luque, P. d. l.: 7Be, 210Pb and 40K depositions over 11 years in Málaga, Journal of Environmental Radioactivity, 178-179, 325-334, https://doi.org/10.1016/j.jenvrad.2017.09.010, 2017.

Dutkiewicz, V. A. and Husain, L.: Stratospheric and tropospheric components of 7Be in surface air, Journal of Geophysical Research: Atmospheres, 90, 5783-5788, 10.1029/JD090iD03p05783, 1985.

Elsässer, C.: Exploration of 10Be ice core records using a climatological model approach: Cosmogenic production versus climate variability, 2013.

Elsässer, C., Wagenbach, D., Weller, R., Auer, M., Wallner, A., and Christl, M.: Continuous 25-yr aerosol records at coastal Antarctica, Tellus B: Chemical and Physical Meteorology, 63, 920-934, 10.1111/j.1600-0889.2011.00543.x, 2011.

Field, C. V., Schmidt, G. A., Koch, D., and Salyk, C.: Modeling production and climate-related impacts on [10]Be concentration in ice cores, Journal of Geophysical Research, 111, 10.1029/2005jd006410, 2006.

Gao, J., Korte, M., Panovska, S., Rong, Z., and Wei, Y.: Effects of the Laschamps Excursion on Geomagnetic Cutoff Rigidities, Geochemistry, Geophysics, Geosystems, 23, e2021GC010261, https://doi.org/10.1029/2021GC010261, 2022.

Gelaro, R., McCarty, W., Suarez, M. J., Todling, R., Molod, A., Takacs, L., Randles, C., Darmenov, A., Bosilovich, M. G., Reichle, R., Wargan, K., Coy, L., Cullather, R., Draper, C., Akella, S., Buchard, V., Conaty, A., da Silva, A., Gu, W., Kim, G. K., Koster, R., Lucchesi, R., Merkova, D., Nielsen, J. E., Partyka, G., Pawson, S., Putman, W., Rienecker, M., Schubert, S. D., Sienkiewicz, M., and Zhao, B.: The Modern-Era Retrospective Analysis for Research and Applications, Version 2 (MERRA-2), J Clim, Volume 30, 5419-5454, 10.1175/JCLI-D-16-0758.1, 2017.

Gfeller, G., Fischer, H., Bigler, M., Schüpbach, S., Leuenberger, D., and Mini, O.: Representativeness and seasonality of major ion records derived from NEEM firn cores, The Cryosphere, 8, 1855-1870, 10.5194/tc-8-1855-2014, 2014.

Golubenko, K., Rozanov, E., Kovaltsov, G., Leppänen, A.-P., Sukhodolov, T., and Usoskin, I.: Application of CCM SOCOL-AERv2-BE to cosmogenic beryllium isotopes: description and validation for polar regions, Geoscientific Model Development, 14, 7605-7620, 10.5194/gmd-14-7605-2021, 2021.

Graham, I., Ditchburn, R., and Barry, B.: Atmospheric deposition of 7Be and 10Be in New Zealand rain
(1996-98), Geochimica et Cosmochimica Acta, 67, 361-373, https://doi.org/10.1016/S0016-7037(02)01092-X,
2003.

Heikkilä, U. and Smith, A. M.: Influence of model resolution on the atmospheric transport of
[10]Be, Atmospheric Chemistry and Physics, 12, 10601-10612, 10.5194/acp-12-10601-2012, 2012.

Heikkilä, U., Beer, J., and Alfimov, V.: Beryllium-10 and beryllium-7 in precipitation in Dübendorf (440 m)
and at Jungfraujoch (3580 m), Switzerland (1998–2005), Journal of Geophysical Research, 113, D11104,
10.1029/2007jd009160, 2008a.

Heikkilä, U., Beer, J., and Feichter, J.: Modeling cosmogenic radionuclides ^{10}Be and ^{7}Be during the Maunder
Minimum using the ECHAM5-HAM General Circulation Model, Atmospheric Chemistry and Physics, 8,
2797-2809, 10.5194/acp-8-2797-2008, 2008b.

Heikkilä, U., Beer, J., Abreu, J. A., and Steinhilber, F.: On the Atmospheric Transport and Deposition of the
Cosmogenic Radionuclides (^{10}Be): A Review, Space Science Reviews, 176, 321-332,
10.1007/s11214-011-9838-0, 2011.

Heikkilä, U., Beer, J., Jouzel, J., Feichter, J., and Kubik, P.: ^{10}Be measured in a GRIP snow pit and modeled
using the ECHAM5-HAM general circulation model, Geophys Res Lett, 35, 10.1029/2007gl033067, 2008c.

Herbst, K., Muscheler, R., and Heber, B.: The new local interstellar spectra and their influence on the
production rates of the cosmogenic radionuclides ^{10}Be and ^{14}C, Journal of Geophysical Research: Space Physics,
122, 23-34, 10.1002/2016ja023207, 2017.

Hernandez-Ceballos, M. A., Cinelli, G., Ferrer, M. M., Tollefsen, T., De Felice, L., Nweke, E., Tognoli, P. V.,
Vanzo, S., and De Cort, M.: A climatology of ^{7}Be in surface air in European Union, J Environ Radioact, 141,
62-70, 10.1016/j.jenvrad.2014.12.003, 2015.

Hernández-Ceballos, M. A., Brattich, E., Cinelli, G., Ajtić, J., and Djurdjevic, V.: Seasonality of ^{7}Be
concentrations in Europe and influence of tropopause height, Tellus B: Chemical and Physical Meteorology, 68,
29534, 10.3402/tellusb.v68.29534, 2016.

Hu, J., Sha, Z., Wang, J., Du, J., and Ma, Y.: Atmospheric deposition of 7Be, 210Pb in Xining, a typical city on
the Qinghai-Tibet Plateau, China, Journal of Radioanalytical and Nuclear Chemistry, 324, 1141-1150,
10.1007/s10967-020-07127-3, 2020.

Huang, J., Kang, S., Shen, C., Cong, Z., Liu, K., Wang, W., and Liu, L.: Concentration and seasonal variation of
10Be in surface aerosols of Lhasa, Tibet, Chinese Science Bulletin, 55, 2572-2578,
10.1007/s11434-010-3233-1, 2010.

Huh, C.-A., Su, C.-C., and Shiau, L.-J.: Factors controlling temporal and spatial variations of atmospheric
deposition of7Be and210Pb in northern Taiwan, Journal of Geophysical Research, 111, 10.1029/2006jd007180,
2006.

Ioannidou, A. and Papastefanou, C.: Precipitation scavenging of ^{7}Be and ^{137}Cs radionuclides in air, J Environ
Radioact, 85, 121-136, 10.1016/j.jenvrad.2005.06.005, 2006.

Jordan, C. E., Dibb, J. E., and Finkel, R. C.: 10Be/7Be tracer of atmospheric transport and
stratosphere-troposphere exchange, Journal of Geophysical Research: Atmospheres, 108,
https://doi.org/10.1029/2002JD002395, 2003.

Koch, D. and Rind, D.: Beryllium 10/beryllium 7 as a tracer of stratospheric transport, Journal of Geophysical Research: Atmospheres, 103, 3907-3917, https://doi.org/10.1029/97JD03117, 1998.

750 Koch, D. M., Jacob, D. J., and Graustein, W. C.: Vertical transport of tropospheric aerosols as indicated by 7Be and 210Pb in a chemical tracer model, Journal of Geophysical Research: Atmospheres, 101, 18651-18666, https://doi.org/10.1029/96JD01176, 1996.

Kong, Y. C., Lee, O. S. M., and Yung, C. H.: Study of the naturally occurring radionuclide Beryllium-7 (Be-7) in Hong Kong, Journal of Environmental Radioactivity, 246, 106850, 755 https://doi.org/10.1016/j.jenvrad.2022.106850, 2022.

Kusmierczyk-Michulec, J., Gheddou, A., and Nikkinen, M.: Influence of precipitation on ^{7}Be concentrations in air as measured by CTBTO global monitoring system, J Environ Radioact, 144, 140-151, 10.1016/j.jenvrad.2015.03.014, 2015.

Lal, D. and Peters, B.: Cosmic Ray Produced Radioactivity on the Earth, in: Kosmische Strahlung II / Cosmic 760 Rays II, edited by: Sitte, K., Springer Berlin Heidelberg, Berlin, Heidelberg, 551-612, 10.1007/978-3-642-46079-1_7, 1967.

Lee, H. I., Huh, C. A., Lee, T., and Huang, N. E.: Time series study of a 17-year record of (7)Be and (210)Pb fluxes in northern Taiwan using ensemble empirical mode decomposition, J Environ Radioact, 147, 14-21, 10.1016/j.jenvrad.2015.04.017, 2015.

765 Leppänen, A. P., Pacini, A. A., Usoskin, I. G., Aldahan, A., Echer, E., Evangelista, H., Klemola, S., Kovaltsov, G. A., Mursula, K., and Possnert, G.: Cosmogenic ^{7}Be in air: A complex mixture of production and transport, Journal of Atmospheric and Solar-Terrestrial Physics, 72, 1036-1043, https://doi.org/10.1016/j.jastp.2010.06.006, 2010.

Liu, H., Jacob, D. J., Bey, I., and Yantosca, R. M.: Constraints from210Pb and7Be on wet deposition and 770 transport in a global three-dimensional chemical tracer model driven by assimilated meteorological fields, Journal of Geophysical Research: Atmospheres, 106, 12109-12128, 10.1029/2000jd900839, 2001.

Liu, H., Jacob, D. J., Dibb, J. E., Fiore, A. M., and Yantosca, R. M.: Constraints on the sources of tropospheric ozone from 210Pb-7Be-O3 correlations, Journal of Geophysical Research: Atmospheres, 109, https://doi.org/10.1029/2003JD003988, 2004.

775 Liu, H., Considine, D. B., Horowitz, L. W., Crawford, J. H., Rodriguez, J. M., Strahan, S. E., Damon, M. R., Steenrod, S. D., Xu, X., Kouatchou, J., Carouge, C., and Yantosca, R. M.: Using beryllium-7 to assess cross-tropopause transport in global models, Atmospheric Chemistry and Physics, 16, 4641-4659, 10.5194/acp-16-4641-2016, 2016.

Liu, X., Fu, Y., Bi, Y., Zhang, L., Zhao, G., Xian, F., and Zhou, W.: Monitoring Surface 10Be/7Be Directly 780 Reveals Stratospheric Air Intrusion in Sichuan Basin, China, Journal of Geophysical Research: Atmospheres, 127, e2022JD036543, https://doi.org/10.1029/2022JD036543, 2022a.

Liu, X., Fu, Y., Wang, Q., Bi, Y., Zhang, L., Zhao, G., Xian, F., Cheng, P., Zhang, L., Zhou, J., and Zhou, W.: Unraveling the process of aerosols secondary formation and removal based on cosmogenic beryllium-7 and beryllium-10, Science of The Total Environment, 821, 153293, https://doi.org/10.1016/j.scitotenv.2022.153293, 785 2022b.

Maejima, Y., Matsuzaki, H., and Higashi, T.: Application of cosmogenic 10Be to dating soils on the raised coral reef terraces of Kikai Island, southwest Japan, Geoderma, 126, 389-399, https://doi.org/10.1016/j.geoderma.2004.10.004, 2005.

Mari, C., Jacob, D. J., and Bechtold, P.: Transport and scavenging of soluble gases in a deep convective cloud,
790 Journal of Geophysical Research: Atmospheres, 105, 22255-22267, https://doi.org/10.1029/2000JD900211, 2000.

Masarik, J. and Beer, J.: Simulation of particle fluxes and cosmogenic nuclide production in the Earth's atmosphere, Journal of Geophysical Research: Atmospheres, 104, 12099-12111, 10.1029/1998jd200091, 1999.

Masarik, J. and Beer, J.: An updated simulation of particle fluxes and cosmogenic nuclide production in the
795 Earth's atmosphere, Journal of Geophysical Research, 114, 10.1029/2008jd010557, 2009.

Méndez-García, C. G., Rojas-López, G., Padilla, S., Solís, C., Chávez, E., Acosta, L., and Huerta, A.: The impact of stable 27Al in 26Al/10Be meteoric ratio in PM2.5 from an urban area, Journal of Environmental Radioactivity, 246, 106832, https://doi.org/10.1016/j.jenvrad.2022.106832, 2022.

Monaghan, M. C., Krishnaswami, S., and Turekian, K. K.: The global-average production rate of 10Be, Earth
800 and Planetary Science Letters, 76, 279-287, https://doi.org/10.1016/0012-821X(86)90079-8, 1986.

Muscheler, R., Joos, F., Beer, J., Müller, S. A., Vonmoos, M., and Snowball, I.: Solar activity during the last 1000yr inferred from radionuclide records, Quaternary Science Reviews, 26, 82-97, 10.1016/j.quascirev.2006.07.012, 2007.

Myers, J. L., Well, A. D., and Lorch Jr, R. F.: Research design and statistical analysis, Routledge2013.

805 Pacini, A. A., Usoskin, I. G., Mursula, K., Echer, E., and Evangelista, H.: Signature of a sudden stratospheric warming in the near-ground [7]Be flux, Atmospheric Environment, 113, 27-31, 10.1016/j.atmosenv.2015.04.065, 2015.

Padilla, S., Lopez-Gutierrez, J. M., Manjon, G., Garcia-Tenorio, R., Galvan, J. A., and Garcia-Leon, M.: Meteoric (10)Be in aerosol filters in the city of Seville, J Environ Radioact, 196, 15-21,
810 10.1016/j.jenvrad.2018.10.009, 2019.

Pedro, J. B., Smith, A. M., Simon, K. J., van Ommen, T. D., and Curran, M. A. J.: High-resolution records of the beryllium-10 solar activity proxy in ice from Law Dome, East Antarctica: measurement, reproducibility and principal trends, Climate of the Past, 7, 707-721, 10.5194/cp-7-707-2011, 2011a.

Pedro, J. B., Heikkilä, U. E., Klekociuk, A., Smith, A. M., van Ommen, T. D., and Curran, M. A. J.:
815 Beryllium-10 transport to Antarctica: Results from seasonally resolved observations and modeling, Journal of Geophysical Research: Atmospheres, 116, 10.1029/2011jd016530, 2011b.

Pedro, J. B., McConnell, J. R., van Ommen, T. D., Fink, D., Curran, M. A. J., Smith, A. M., Simon, K. J., Moy, A. D., and Das, S. B.: Solar and climate influences on ice core [10]Be records from Antarctica and Greenland during the neutron monitor era, Earth and Planetary Science Letters, 355-356, 174-186,
820 10.1016/j.epsl.2012.08.038, 2012.

Poluianov, S. V., Kovaltsov, G. A., Mishev, A. L., and Usoskin, I. G.: Production of cosmogenic isotopes [7]Be, [10]Be, ^{14}C, [22]Na, and [36]Cl in the atmosphere: Altitudinal profiles of yield functions, Journal of Geophysical Research: Atmospheres, 121, 8125-8136, 10.1002/2016jd025034, 2016.

Raisbeck, G. M., Yiou, F., Fruneau, M., Loiseaux, J. M., Lieuvin, M., and Ravel, J. C.: Deposition rate and
825 seasonal variations in precipitation of cosmogenic 10Be, Nature, 282, 279-280, 10.1038/282279a0, 1979.

Raisbeck, G. M., Yiou, F., Fruneau, M., Loiseaux, J. M., Lieuvin, M., and Ravel, J. C.: Cosmogenic [10]Be/[7]Be as a probe of atmospheric transport processes, Geophys Res Lett, 8, 1015-1018, 10.1029/GL008i009p01015, 1981.

Rodriguez-Perulero, A., Baeza, A., and Guillen, J.: Seasonal evolution of [7,10]Be and [22]Na in the near surface atmosphere of Caceres (Spain), J Environ Radioact, 197, 55-61, 10.1016/j.jenvrad.2018.11.015, 2019.

830   Sangiorgi, M., Hernández Ceballos, M. A., Iurlaro, G., Cinelli, G., and de Cort, M.: 30 years of European Commission Radioactivity Environmental Monitoring data bank (REMdb) – an open door to boost environmental radioactivity research, Earth System Science Data, 11, 589-601, 10.5194/essd-11-589-2019, 2019.

Smart, D. F. and Shea, M. A.: A review of geomagnetic cutoff rigidities for earth-orbiting spacecraft, Advances
835   in Space Research, 36, 2012-2020, https://doi.org/10.1016/j.asr.2004.09.015, 2005.

Somayajulu, B. L. K., Sharma, P., Beer, J., Bonani, G., Hofmann, H. J., Morenzoni, E., Nessi, M., Suter, M., and Wölfli, W.: 10Be annual fallout in rains in India, Nuclear Instruments and Methods in Physics Research Section B: Beam Interactions with Materials and Atoms, 5, 398-403, https://doi.org/10.1016/0168-583X(84)90549-4, 1984.

840   Sukhodolov, T., Usoskin, I., Rozanov, E., Asvestari, E., Ball, W. T., Curran, M. A., Fischer, H., Kovaltsov, G., Miyake, F., Peter, T., Plummer, C., Schmutz, W., Severi, M., and Traversi, R.: Atmospheric impacts of the strongest known solar particle storm of 775 AD, Sci Rep, 7, 45257, 10.1038/srep45257, 2017.

Terzi, L. and Kalinowski, M.: World-wide seasonal variation of [7]Be related to large-scale atmospheric circulation dynamics, J Environ Radioact, 178-179, 1-15, 10.1016/j.jenvrad.2017.06.031, 2017.

845   Terzi, L., Kalinowski, M., Schoeppner, M., and Wotawa, G.: How to predict seasonal weather and monsoons with radionuclide monitoring, Sci Rep, 9, 2729, 10.1038/s41598-019-39664-7, 2019.

Uhlar, R., Harokova, P., Alexa, P., and Kacmarik, M.: (7)Be atmospheric activity concentration and meteorological data: Statistical analysis and two-layer atmospheric model, J Environ Radioact, 219, 106278, 10.1016/j.jenvrad.2020.106278, 2020.

850   Usoskin, I. G., Field, C. V., Schmidt, G. A., Leppänen, A.-P., Aldahan, A., Kovaltsov, G. A., Possnert, G., and Ungar, R. K.: Short-term production and synoptic influences on atmospheric [7]Be concentrations, Journal of Geophysical Research, 114, D06108, 10.1029/2008jd011333, 2009.

Villarreal, R. E., Arazi, A., and Fernandez Niello, J. O.: Correlation between the latitudinal profile of the (7)Be air concentration and the Hadley cell extent in the Southern Hemisphere, J Environ Radioact, 244-245, 106760,
855   10.1016/j.jenvrad.2021.106760, 2022.

Wang, Q., Jacob, D. J., Fisher, J. A., Mao, J., Leibensperger, E. M., Carouge, C. C., Le Sager, P., Kondo, Y., Jimenez, J. L., Cubison, M. J., and Doherty, S. J.: Sources of carbonaceous aerosols and deposited black carbon in the Arctic in winter-spring: implications for radiative forcing, Atmos. Chem. Phys., 11, 12453-12473, 10.5194/acp-11-12453-2011, 2011.

860   Waugh, D. and Hall, T.: Age of Stratospheric Air: Theory, Observations, and Models, Reviews of Geophysics, 40, 1-1-1-26, 10.1029/2000rg000101, 2002.

Yamagata, T., Nagai, H., Matsuzaki, H., and Narasaki, Y.: Decadal variations of atmospheric [7]Be and [10]Be concentrations between 1998 and 2014 in Japan, Nuclear Instruments and Methods in Physics Research Section B: Beam Interactions with Materials and Atoms, 455, 265-270, https://doi.org/10.1016/j.nimb.2018.12.029,
865   2019.

Zhang, B., Liu, H., Crawford, J. H., Chen, G., Fairlie, T. D., Chambers, S., Kang, C. H., Williams, A. G., Zhang, K., Considine, D. B., Sulprizio, M. P., and Yantosca, R. M.: Simulation of radon-222 with the GEOS-Chem global model: emissions, seasonality, and convective transport, Atmos. Chem. Phys., 21, 1861-1887, 10.5194/acp-21-1861-2021, 2021a.

870 Zhang, F., Wang, J., Baskaran, M., Zhong, Q., Wang, Y., Paatero, J., and Du, J.: A global dataset of atmospheric ^{7}Be and ^{210}Pb measurements: annual air concentration and depositional flux, Earth System Science Data, 13, 2963-2994, 10.5194/essd-13-2963-2021, 2021b.

Zheng, M., Liu, H., Adolphi, F., Muscheler, R., Lu, Z., Wu, M., and Prisle, N. L.: Simulations of 7Be and 10Be with the GEOS-Chem global model v14.0.2 using state-of-the-art production rates, Zenodo, 875 10.5281/zenodo.8051729, 2023.

Zheng, M., Sjolte, J., Adolphi, F., Aldahan, A., Possnert, G., Wu, M., and Muscheler, R.: Solar and meteorological influences on seasonal atmospheric ^{7}Be in Europe for 1975 to 2018, Chemosphere, 263, https://doi.org/10.1016/j.chemosphere.2020.128318, 2021a.

Zheng, M., Adolphi, F., Sjolte, J., Aldahan, A., Possnert, G., Wu, M., Chen, P., and Muscheler, R.: Solar and 880 climate signals revealed by seasonal ^{10}Be data from the NEEM ice core project for the neutron monitor period, Earth and Planetary Science Letters, 541, https://doi.org/10.1016/j.epsl.2020.116273, 2020.

Zheng, M., Adolphi, F., Sjolte, J., Aldahan, A., Possnert, G., Wu, M., Chen, P., and Muscheler, R.: Solar Activity of the Past 100 Years Inferred From ^{10}Be in Ice Cores—Implications for Long-Term Solar Activity Reconstructions, Geophys Res Lett, 48, e2020GL090896, https://doi.org/10.1029/2020GL090896, 2021b.

885